Lumbar Spine Injury Assessment of Frontal Crash Occupants: Translating HBM Metrics to THOR ATDs

Sophia K. Tushak, Katarzyna Rawska, Jason R. Kerrigan, Adrian Felix Caudillo-Huerta, Bronislaw Gepner

Abstract Lumbar spine injuries have been observed in PMHS sled tests and field data, yet no ATD lumbar injury criteria currently exist in vehicle regulation. This study quantified lumbar loading in matched THOR–HBM frontal crash simulations and assessed force and moment relationships for translating human lumbar injury risk to ATDs, using HBMs as a bridge. The matched simulation matrix varied ten parameters known/hypothesised to influence lumbar loading, including delta-v, seat, restraints, and posture. From these, 84 non-submarining matched cases were identified for comparison. Peak compression forces, and some peak flexion moments, were linearly correlated, with relationships varying for each HBM-THOR comparison. The GHBMC Lfx injury metric predicted among the highest injury risk at the T12 vertebrae, consistent with PMHS and field data, aligning ATD predictions with the anatomical location of the loadcell. This alignment enables direct comparison of loads between PMHS, HBMs, and ATDs, supporting the use of ATD lumbar loadcell data to assess occupant injury risk in future vehicles. This is the first study to systematically evaluate multiple THOR variants and HBMs regarding lumbar spine loading under varied frontal impact conditions, establishing foundational relationships for translating HBM-based lumbar injury metrics derived from human data to ATDs.

Keywords Anthropomorphic test devices, Human body models, Lumbar spine injury, Matched simulations, Parametric study.

I. INTRODUCTION

Frontal crashes have historically elicited a higher proportion of AIS2+ lumbar spine fractures (e.g., compression, wedge, burst types) than other crash directions [1–2], and have also been identified in frontal sled tests with post-mortem human subjects (PMHS) [3–13]. These fracture types have been linked to compression loading with and without flexion via biological experimentation [14–18]. Further, field crash data [1][19–20] have shown that occupants in frontal crashes sustain a relatively high rate of lumbar spine fractures resulting from compression and compression combined with flexion bending. PMHS-derived and human body model (HBM)-derived (specifically for the 50th percentile male GHBMC) injury risk functions (IRFs) that can be used to predict lumbar spine fracture in compression or in compression-flexion dynamic loading analogous to that experienced during potentially injurious frontal crashes have been developed and presented in the biomechanics literature [21–23].

However, there are presently no standards for quantifying acceptable lumbar spine loads and injury risk in vehicle regulation. Moreover, there have not yet been any studies in open literature pertaining to quantification and interpretation of spinal loads from anthropomorphic test devices (ATDs) in frontal sled tests, and how they relate to human injury risk. Injury risk prediction with ATDs is a fundamental and critically important aspect of vehicle safety evaluation used in both government compliance and consumer-information testing. Since ATDs have limited instrumentation and varying materials, PMHS-derived injury risk prediction typically needs to be translated or transformed to provide relevant predictions in ATDs. Moreover, the simplification in design and intended use of dummies relative to human tissues affect the measured kinematics and kinetics from both physical ATDs and their computational counterparts across the loading cases in which they are assessed. For example, spinal loads are measured in one or two load cells placed in anatomically equivalent locations that are in series with one rubber joint assumed to represent and modulate the deformation of the entire spinal column. Whereas, humans, and their computational counterparts human body models (HBMs), contain five lumbar spine

S. K. Tushak (e-mail: skt5ay@virginia.edu) was a PhD student while completing this research; K. Rawska is a Senior Lab Specialist; J. R. Kerrigan is a Professor; A. F. Caudillo-Huerta is a Research Engineer; and B. D. Gepner is an Assistant Research Professor, all at the University of Virginia's Center for Applied Biomechanics in the Department of Mechanical and Aerospace Engineering, Charlottesville, USA.

vertebrae between flexible intervertebral discs with seemingly infinite measurement locations in which to place instrumentation. Additionally, the ATD spine was likely designed to be stiffer than human spines because it must facilitate torso pitch in the absence of load sharing with soft tissue (i.e., the ATD abdominal foam and jacket cannot bear as much load as human soft tissues), so direct application of PMHS-derived injury risk prediction is likely not appropriate. Given the difficulty in measuring spinal loads in PMHS sled tests, HBMs can be explored as a way to interpret loading in the human and then be linked to virtual ATDs. Computational models present a unique opportunity to examine the spinal loading relationships between surrogates given variations in crash, vehicle, and occupant parameters. Further, if the HBM and ATD display similar relationships in spinal loading behavior, injury risk prediction may be transferred to the ATD. Thus, HBMs may facilitate the development of dummy injury criteria across a multitude of frontal impact scenarios.

HBM simulation studies have suggested that lumbar spine forces and moments are affected by several occupant and environmental factors. Lumbar spine injuries have been reported at impact speeds ranging from around 35–60 km/h [1–2][19][24–27] and have been attributed to higher impact speeds [5][20]. Spine loads have been shown to increase when the occupant's torso is initially reclined closer to horizontal [6][9][28–34]. Further, initial spinal curvature has been suggested to affect lumbar spine loading, in which slouched postures result in higher lumbar spine loading [28] and more lumbar spine fractures [36]. Additionally, it is hypothesised that lumbar spine forces and moments are also affected by load sharing between the lumbar spine and surrounding load paths in the lower thorax and abdomen. If the tissue surrounding the spine had negligible stiffness, then the compressive load would be borne entirely by the spine. Certain aspects of restraint systems, such as load limiting and belt take-off angle, may affect lumbar spine loading and may be able to be optimised. Restraining the pelvis such that minimal pelvis excursion occurs has been suggested to result in higher magnitudes of loading to be propagated from the seat to the lumbar spine [37], while submarining has been found to off-load the lumbar spine [30]. Conversely, load limiting of the seat track, seat pan, and lap belt have been shown to reduce lumbar spine loading [38]. Additionally, the type of seat and its inherent properties (stiffness, cushioning, etc.) has been shown to affect the magnitude of loading to the lumbar spine [8][35]. Lastly, the use of a knee bolster is hypothesised to introduce an alternative load path for energy transfer during an impact. Given the frequency of lumbar spine injuries in the field, the risks predicted for reclined occupants, and the known or hypothesised effects of other factors identified to vary among occupants and vehicles, the transformation of injury risk prediction from the human to the dummy via HBMs should be timely and prove robust to these considerations.

Therefore, the goal of this study was to quantify the relationships between HBM and dummy loads in matched frontal crash boundary conditions across a range of intrinsic and extrinsic parameters. The aim was to compare lumbar spine loads from several THOR FE models that are designed for both traditional upright seating postures (THOR-50M) and include modifications for reclined seating (THOR-RS and THOR-AV) to those from HBMs to provide insight into the plausibility of using a HBM to link human lumbar injury risk to THOR lumbar spine injury risk.

II. METHODS

Whole body sled tests were simulated with various combinations of discretised (1) torso angle, (2) pelvis-spine orientation, (3) flesh stiffness, (4) organ stiffness, (5) impact speed, (6) restraint functionality, (7) lap belt anchorage position, (8) shoulder belt angle, (9) seat type, and (10) knee bolster use. These factors have been found to affect lumbar spine loading and injury rates in previous studies with PMHS, computational models, and crash investigation data, or were hypothesised to affect such loads. Fiftieth-percentile male computational models were utilised; two of which have been specifically developed to investigate reclined postures. The Total HUman Model for Safety (THUMS; v7), Global Human Body Models Consortium (GHBMC; v6.0), and four variations of the Test device for Human Occupant Restraint (THOR; 50M-UVA-NHTSA v2.8; 50M-ATD-MODELS v1.05; RS v1.05 from ATD-MODELS; AV v0.7.2 from Humanetics) were simulated in matched boundary conditions for one-to-one comparisons. These models were first simulated in a baseline case using exact PMHS and THOR positioning data and compared to their in-lab sled test counterparts [6][9][29][39–41], except for THOR-AV since no physical sled test had been performed. Models were then parameterised from this baseline case, as described in later sub-sections. The HBMs and THOR 50M-UVA-NHTSA results come from a previously executed study, whereas THOR 50M-ATD-MODELS, RS, and AV were simulated specifically for the purpose of this study. Any differences between the first and second sets of simulations will be pointed out and explained in later sub-sections.

It should be noted that the designs of THOR-RS and THOR-AV deviate from the traditional THOR-50M. Namely in the spine, THOR-RS replaced the rigid spine pitch mechanism with a flexible joint (two flexible joints total), and THOR-AV included a wedge part in the neck and altered lower thoracic pitch adjustment design to aid in positioning to extreme recline angles [42–43]. The THOR-AV model release included three pre-positioned models, including 25° (with a 12° superslouch spine pitch), 45° (with a -6° erect spine pitch), and 65° (with a -15° super-erect spine pitch) torso angles. The 45° and 65° positions include an abdominal wedge part to achieve the torso and spine orientations. For the purposes of the current study and to exactly match the parameter levels of the previous study, the 25° (with a 12° superslouch spine pitch and no abdominal wedge part) model was used and re-positioned to the other target postures, as described in future sections.

In general, stresses and strains were removed from all pre-simulations. Simulations were performed on the UVA High Performance Computing Cluster using LS-Dyna Massively Parallel Processing (MPP) explicit FE solver (R9.3.1 for the first set of simulations and R12.2.1 for the second set of simulations, both in single-precision MPP971—consistency between both versions was ensured by re-simulating select cases), with a run time of 160 ms. Simulations not reaching 95 ms in duration were removed from further analysis, as they were not inclusive of peak lumbar spine compression forces and flexion moments. Simulations resulting in submarining were also removed from further analysis since submarining has been shown to off-load the lumbar spine [30].

Factor Sampling and Parameterisation

The ten factors were varied at two to four levels (Table 1). Selected levels of parameters were chosen to study lumbar spine loading when submarining does not occur. Thus, values of parameter levels were chosen to avoid the risk of submarining, with some based on findings from a previous study [44].

TABLE I
Factors selected for analysis. Bolded levels indicate Baseline Case conditions that matched previous reclined occupant sled tests [6][9]. Unbolded levels indicate iteration from the baseline, often in a direction that aimed to avoid submarining.

Factor	Levels
Delta-V	Slower (40 km/h)
	Faster (51 km/h)
Restraint Type	**3PT + 3.5kNSBLL (1)**
	3PT + 2.5kNSBLL (2)
	3PT + 3.5kNSBLL + 5+7kNLBLL (3)
	2PT + 3.5kNSBLL (4)
Knee Bolster	On (Included)
	Off (Excluded)
Seat Type	**Semi-rigid**
	Vehicle
Lap Belt Anchor Position	**Nominal (0 mm)**
	Forward (+52 mm)
Shoulder Belt Take-Off Angle	**Positive (+12°)**
	Negative (-12°)
Pelvis Angle (Lumbar Orientation)	**Nominal (0°)**
	Posterior (12°)
Recline Angle	Upright (25°)
	Reclined (50°)
	Highly Reclined (60°)
Flesh Stiffness	**Nominal (1x SF)**
	Stiffer (5x SF)
Organ Stiffness	**Nominal (1x SF)**
	Stiffer (5x SF)

Eight of the variables were discretised to two levels, with precise values based on literature and/or current vehicle regulation standards. In the second set of simulations with THOR 50M-ATD-MODELS, RS, and AV, the flesh and organ stiffness for the THOR analog were not varied, and only nominal/stock values were utilised. Firstly, these two parameters were found not to substantially influence lumbar spine loads in the first set of simulations with the HBMs and THOR 50M-UVA-NHTSA. Additionally, and importantly, the material characteristics of these dummy parts are encrypted within the commercial models used in this study, restricting direct modification by the user. Factor levels are discussed in later relevant sub-sections and Appendix A.

A full-factorial simulation study was not feasible, as it would have required 3,072 simulations. Thus, sub-sampling reduced the number to 192 sled-style frontal impact simulations per surrogate (Eq. A1). A sixteenth fractional factorial design with a resolution of IV was introduced for the eight variables sampled at two levels, resulting in 16 runs [45]. The resulting sampling scheme pre-allocated combinations of factor levels such that each factor was equally sampled, and information of the entire parameter space was gained via Design of Experiments (see Appendix A). The sixteenth fractional-factorial was applied within each combination of torso angle (three levels) and restraint type (categorical, four levels).

Environment

The environment model included a publicly available, generic, tunable restraint model [46]. The seat-belt restraint anchor positions were symmetrically mirrored to obtain a passenger orientation, replicating previous reclined occupant sled tests and simulations [6][9][29][39–40]. The functionality and anchor positions were tuned to match reclined sled tests and simulations conducted by UVA and Autoliv [6][9][29][39–40]and were designed to mitigate potential submarining, including triple pretensioning and shoulder belt load limiting. The shoulder belt D-ring and B-pillar mimicked a belt-in-seat structure. The lap belt included a buckle with crash-locking tongue, which allowed for slip through the belt during pretensioning, but none thereafter. See Appendix A for description of restraint modifications to achieve the desired factor levels. The knee bolster restraint included foam reinforced with a metal structure, and its position was not changed from the stock restraint model (see Fig. B4 for example).

Two seat models were included. The semi-rigid seat model, designed to approximate the stiffness of vehicle seats [36], was tuned to replicate functionality of previous reclined occupant sled tests and simulations[6][9][29][39–40], with the deformable seat pan angled at 15° and anti-submarining ramp angled at 30° from the horizontal. Additionally, a publicly available 2010-2012 Toyota Auris vehicle seat model was included (25° seatback, mid-height headrest location, approximately 13° seat pan angle) [47]. Nominal anchorage positions for the semi-rigid seat were based on physical test boundary conditions [6][9]. H-point design specifications were used to equate restraint anchor positions between the native semi-rigid seat and vehicle seat with respect to the rotational axes of both seats, so that the relative position of the belt anchorages to the design H-point was the same with both seat models (see Appendix A for more). A slow (40 k/hr) or fast (51 k/hr) delta-v was applied (see Appendix A for more).

Occupant Positioning

Torso angle was discretised to three levels which represented current and potential future postures occupants may choose in vehicles (upright ≈ 25°, reclined ≈ 50°, and highly reclined ≈ 60°) (Fig. 1). The nominal upright positions were those matched to the stock HBMs due to lack of any other physical sled test positioning targets. The HBM nominal reclined position, obtained from previous PMHS tests [6] and HBM simulations [29][39], has been extensively documented. The virtual THOR nominal recline position matched that of the physical THOR [40–41] via the Oasys Primer (v21.0) positioning tree and displacement cable pre-simulation method using digitised targets from a 3D coordinate measurement machine from physical THOR tests, which was originally estimated from the average PMHS [6]. The spine pitch angle was adjusted to super-slouch (12°) to reflect physical tests (to match both pelvis and torso angles). Key positioning targets for the nominal recline posture included the fore-aft (X) and vertical (Z) location of the H-Point, heel, knee, acromion, head CG, sternum and elbow, as well as spine and pelvis tilt sensor sagittal angles.

The nominal highly reclined position was an exploratory torso angle obtained via the ratio of Nyquist pelvis angles (angle between the vector connecting the ASIS to pubic symphysis and the horizontal in the sagittal plane) between the upright to recline postures, which was used to linearly extrapolate to the highly reclined pelvis angle. The Nyquist angle for upright was approximately 132° for HBMs and 114° for THOR and increased to 162° for

HBMs and 142° for THOR in the reclined posture. The ratio of a 1.2° and 1.12° increase in Nyquist angle for every 1° increase in torso angle resulted in a target of 174° for HBMs and 153° for THOR in highly reclined.

At each HBM torso angle, the nominal lumbar-pelvis orientation was then altered to consider a second orientation in which the pelvis was posteriorly rotated. The value of 12° was arbitrarily determined using static positioning data for volunteers situated in reclined postures [48] (15° standard deviation among pelvis angles) as well as considering the variation of initial pelvis notch angle of the PMHS tests [6] (10° range). The notch angle was defined as the angle between the ASIS-AIIS vector and the horizontal. From the nominal position at each torso angle, the whole HBM was rigidly rotated by 12° rearward about the H-point, and then the same targets and methods for the head, spine, legs, and arms positions were carried out to slouch the lumbar spine while constraining the pelvis.

THOR models included a spine pitch adjustment mechanism (except THOR-RS), which is the only degree of freedom for altering spinal posture. For all THOR models except THOR-RS, the alternative factor level was selected as the "neutral" pitch adjuster position (0°) and was obtained by anteriorly rotating the pelvis (approximately 5°), while maintaining the same H-point position and torso angle as nominal posture (i.e., super-slouch 12°). The neutral pitch adjustment location, with relative anteriorly-rotated pelvis, was matched to the nominal HBM pelvis-spine position, and the super-slouch pitch adjustment location with relative posteriorly-rotated pelvis was matched to the posteriorly-rotated HBM pelvis position, both without any pre-flexion of the THOR spine flexible joints. Due to THOR-RS replacing the spine pitch adjustment mechanism with a flexible joint, two spine pitch postures were not utilised for THOR-RS. For the one spine posture, pre-flexion was incorporated into both THOR-RS flexible spine joints in order to match the tilt angles from the physical sled tests and carried the same amount of pre-flexion to the two other torso angles. The magnitude of pre-flexion totaled 9°s, of which was evenly split between the two flexible joints. Lastly, positioning targets were not available for THOR-AV, therefore spinal joint deformation was matched to that of the THOR-50M, and the flexible spinal joint was kept in an undeformed state across all torso angles. The same relative angles of the arms, legs, and neck were maintained for all torso angles and pelvis-spine orientations of each surrogate model.

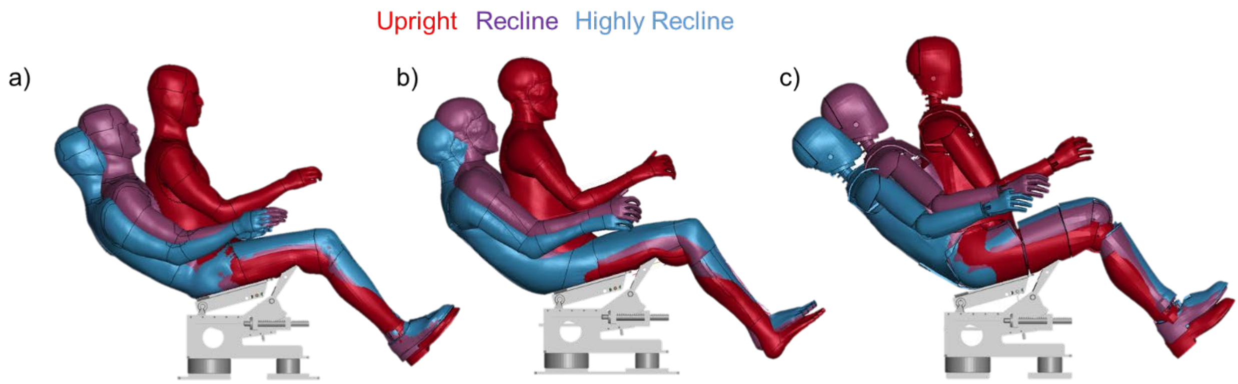

Fig. 1. Example positions for all torso angles for (a) GHBMC, (b) THUMS, and (c) THOR.

Settling and Belt Routing

After obtaining the six positions (three torso angles x two pelvis/spine orientations), the surrogates were settled onto both seats (Fig. 2). The models were settled by prescribing motion to achieve matched H-point positions relative to the physical counterparts. To do so, the skeleton was rigidly constrained to maintain the achieved postures, and the buttock flesh compressed against the seats. For the semi-rigid seat, the HBMs naturally sat 20 mm higher than PMHS when gravity-settled, so the HBMs were forced into the seat by compressing the buttock flesh because it has been shown to improve the pelvis kinematic biofidelity [39]. THOR fore-aft H-point position was matched to physical THOR recline tests [40–41]. The physical THOR sat approximately 35 mm forward and 30 mm above the average H-point location of the PMHS (PMHS final position was approximately 10 mm behind the target H-point position). Further, THOR generally tends to sit higher and forward in seats due to the stiffness, thickness, and geometry of the buttock flesh. As a result, the National Highway Transportation Safety Administration's (NHTSA's) THOR positioning procedure specifies that the THOR H-point should be placed 20 mm forward and 20 mm above the OSCCAR positioning tool reference H-point location [49]. On the other hand, since vertical buttock height of the THOR-RS was modified to better match PMHS (i.e., vertical pelvis flesh was removed), the z-component of THOR-RS's H-point position, when set at the same x-component as THOR-50M, was closer to that from the PMHS and HBMs. The H-point positions of all six postures of each surrogate were the same.

For the vehicle seat, the H-point fore-aft x-position was based on the seat design specifications included with the open-source model while taking positioning requirements into account for THOR, as described above. The vertical position was determined by gravity settling since HBM/THOR and PMHS/THOR flesh differences on the seat cushion could not be similarly identified to those identified on the semi-rigid seat. A contact was not defined between the models and the seatback in order to maintain the six achieved postures. Initial stresses and strains from the settling procedures were not carried through to the final simulations. Static and dynamic coefficients of friction of 0.35 were defined between the surrogate and seatpan entities, which are typical values for automotive impact simulations and have been used in similar studies with the Semi-Rigid seat and advanced restraint [29][39]. The seat belts were semi-automatically routed (Oasys Primer v21.0). Belt routing for vehicle seat cases was allowed to intersect with the seatpan and seatback, as the intended restraint parameter values were to be maintained and only seatpan stiffness and structure were to be varied. A contact was not defined between restraint and seat entities, so this did not affect the functionality of the restraint. Additionally, a contact with static and dynamic coefficients of friction of 0.30 was defined between the surrogates and belts, which are typical values for automotive impact simulations and have been used in similar studies with the Semi-Rigid seat and advanced restraint systems [29][39].

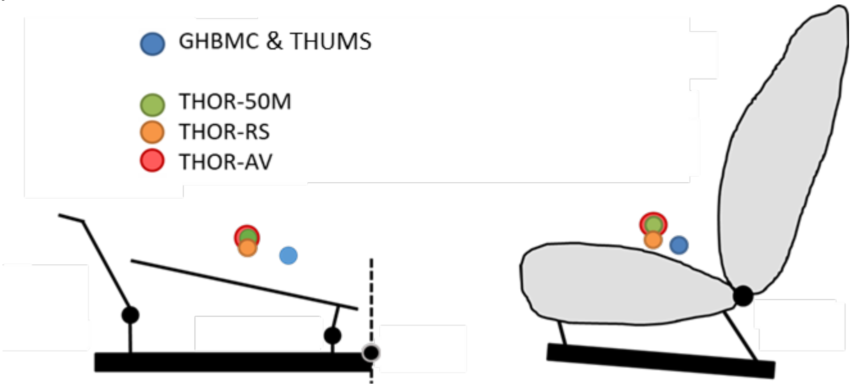

Fig. 2. H-point target positions for all surrogates sitting on the semi-rigid seat (left) and vehicle seat (right).

Submarining Detection

Submarining has been suggested to reduce lumbar spine loading [30], and parameter levels were biased away from submarining, but submarining was still predicted to occur. Variables not yet assessed in the context of submarining, such as seat type and a highly reclined posture, were included and were hypothesised to result in some submarining. Submarining detection was performed using a previously developed method [44]. At each time step, the Euclidean distance between the nodes on the lower edge of the lap belt and the left, right, and middle ASIS nodes were calculated. Concurrently, the lap belt node closest in distance to each of the three ASIS nodes at each time step was quantified. If any of those three lap belt nodes translated above and rearward relative to the ASIS in the global coordinate frame, the simulation was flagged for submarining and removed from further evaluation. Simulations were categorised as submarining regardless of when submarining occurred and if submarining was unilateral or bilateral. Cases resulting in submarining were removed from further analysis.

Lumbar Spine Loads

Peak lumbar spine loads (axial compression forces and flexion bending moments) were recorded at each level from T12 to L5 (HBMs) or the thoracic spine load cell (THOR) (Fig. 3). Further, HBM loads were also analysed using the lumbar level in which the overall peak load occurred, which hypothetically indicated the most injurious level. The thoracolumbar junction, particularly at T12, has reported relatively high prevalence of fractures in the field [1] and PMHS sled tests [3–4][6][8–9][12] and is the representative anatomical location for the inferior-most THOR load cell. Thus, a cross-section at T12 was included, although T12 is not technically considered part of the lumbar spine, it is for this study. Loads were locally recorded at each cross-section (HBMs, THOR-AV) or beam element (both THOR-50M and THOR-RS) with respect to level-specific coordinate systems with SAE reference frame axes (x: forward, y: right, z: down). THOR loads were filtered according to SAE J211 standard to reduce high-frequency noise.

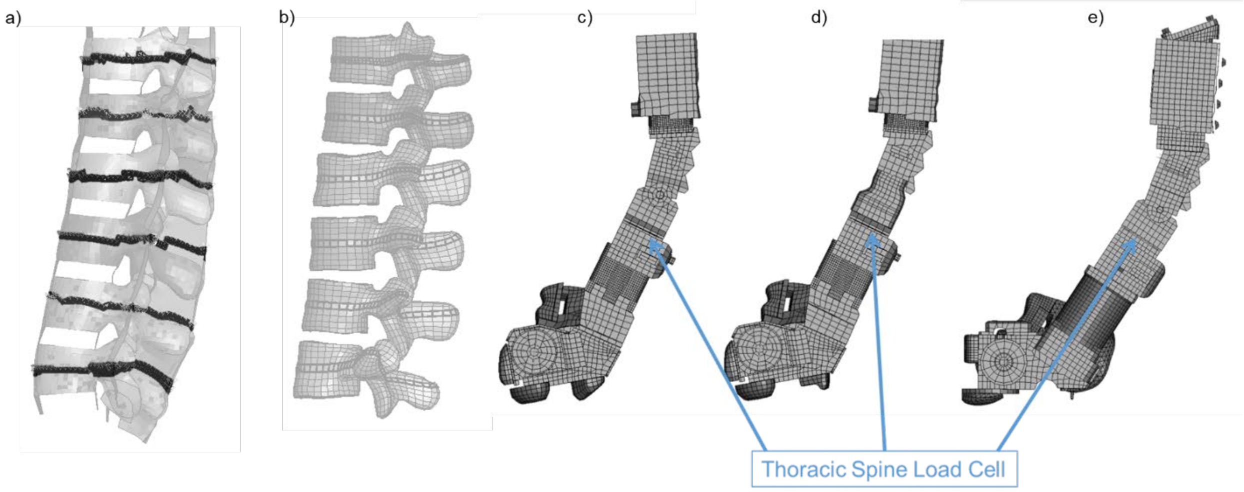

Fig. 3. Definitions of lumbar spine instrumentation, including cross-sections at each T12-L5 vertebral level in the (a) THUMS and (b) GHBMC, and the beam element representing the spine load cell in (c) THOR-50M, (d) THOR-RS, and (e) THOR-AV.

Endplate nodes of interest were tracked in the 3D global coordinate frame for HBMs (Fig. 4). The mid-point of all four endplate nodes was iteratively calculated over time to represent the location of the geometrical centre of the vertebral body. The flexion moment measured at the cross-section centroid was transformed to the vertebral body centre using the Euclidean distance between each vertebral body centre and cross-section centroid (i.e., moment arm) and local axial compression [2]1[50]. This corrected flexion moment will be referred to as the “flexion moment” for this study.

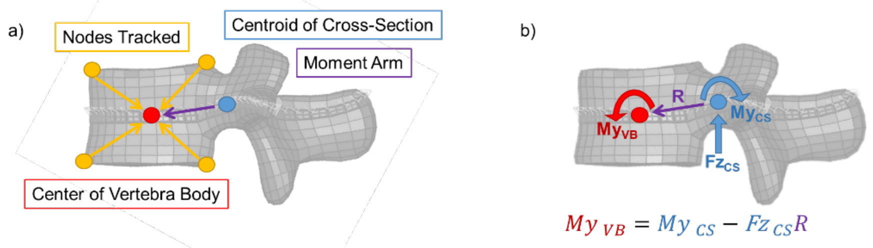

Fig. 4. HBM flexion moment definition, which utilised (a) tracked nodes to calculate the moment arm between the geometrical centre of the vertebral body and the vertebrae cross-section centroid. The moment arm and compression force through the centroid was then used to (b) calculate flexion moment at the vertebral body centre.

Probability of Injury (GHBMC Only)

The highest loads do not always correlate to the highest stresses and highest risk for injury, as cross-sectional area increases superior-to-inferior in the HBMs, and generally in humans. Additionally, peak compression forces and peak flexion moments occurred out-of-phase from each other, and it is possible that one or the other, or sometime in between, is the most injurious point during the crash event. Thus, the GHBMC-specific injury risk function developed by [23] that stemmed from PMHS experimentation [21–22] was utilised to calculate injury risk for GHBMC simulations in this study. The input metric, Lfx, was a function of the linear combination of compression force and flexion moment at each time point, both normalised by vertebral body area to represent a pseudo stress within the lumbar column. Similar injury risk prediction has not been developed for THUMS, so this was only performed on GHBMC simulations.

Statistical Analysis

All statistical analysis was performed using MATLAB (R2018b) with data from non-submarining simulations reaching 95 ms in duration or later. A significance level of 0.05 was utilised. Peak axial compression forces and flexion bending moments were related among surrogates, in total and stratified by levels of each parameter, for the matched cases. Linear fit lines and R^2 were included, and the confidence of the slope coefficient was tested via regression for the range of available data (i.e., not forced to cross through the origin). In the regressions, HBM compression force, HBM flexion moment, or GHBMC probability of injury was the independent variable and THOR compression force or bending moment was the response variable. Test results with $p<0.05$ confirmed slope coefficients significantly greater or less than zero, representing confidence of either positive or negative relationships between HBM loads and THOR loads. Coefficients close to zero with $p>0.05$ represented large variation in HBM and/or THOR data, or insensitivity of HBM loads relative to THOR loads.

III. RESULTS

Of the 192 matched cases that were simulated per surrogate, 84 remained for comparisons after removing those that terminated prior to the critical time of lumbar loading (95 ms) and those that submarined in one or more surrogates. Peak axial compression forces occurred at approximately 60 ms, whereas peak flexion bending moments occurred at approximately 90 ms (see Appendix B for general loading time-duration curves).

THOR 50M-UVA-NHTSA and THOR 50M-ATD-MODELS peak compression forces ranged from approximately 2 to 8 kN; THOR-AV peak compression forces ranged from roughly 2 to 13 kN; THOR-RS peak compression forces ranged from approximately 2 to 6 kN; HBM peak compression forces ranged from approximately 2.2 to 4.7 kN (Fig. 5). THOR 50M-UVA-NHTSA and THOR 50M-ATD-MODELS peak flexion moments ranged from approximately 100 to 500 Nm; THOR-AV peak flexion moments ranged from approximately 200 to 700 Nm; THOR-RS peak flexion moments ranged from approximately 100 to 300; HBM peak flexion moments ranged from approximately 20 to 100 Nm. Many of the data comparing 1) THOR 50M-UVA-NHTSA and THOR 50M-ATD-MODELS and 2) GHBMC to THUMS indicated nearly one-to-one relationships between surrogate compression forces and flexion moments.

The six human surrogates displayed similar directionality in overall peak compression forces, with higher HBM compression forces significantly correlating to higher THOR compression forces (Fig. 5, Table B1). All THOR models generally recorded higher peak compression forces compared to both HBMs, except THOR-RS. When comparing HBM flexion moments to THOR flexion moments, the linear fits were nearly flat and not significant for THUMS, except for THOR-RS, indicating insensitivity of THUMS and THOR across the wide range of parameters and wide range in recorded THOR flexion moments (Fig. 5, Table B1). GHBMC flexion moments were significantly negatively associated with THOR flexion moments, except THOR-RS, which was significantly positively related to THOR flexion moments but had a slope close to one. All THOR flexion moments were above the y=x line and higher than the HBM flexion moments recorded in the matched case.

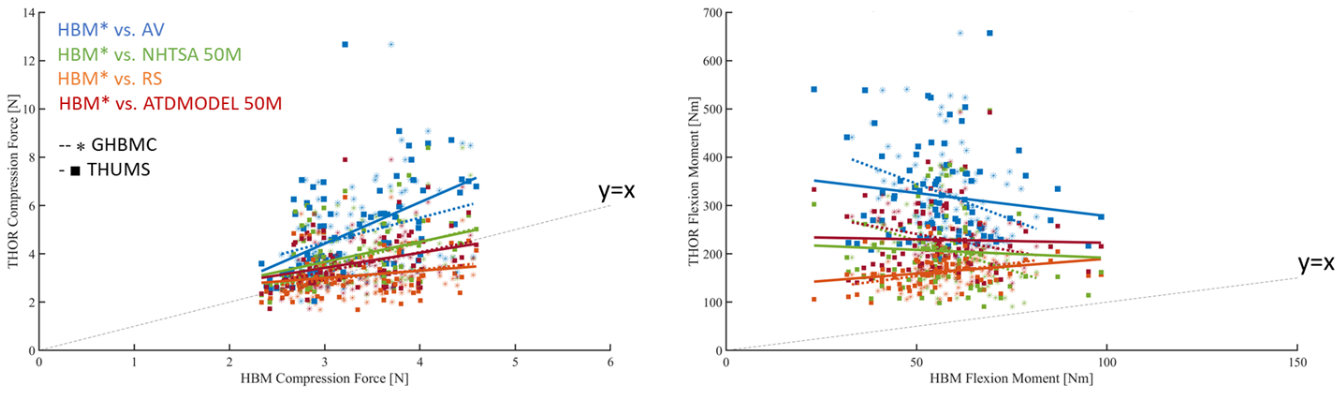

Fig. 5. Peak compression force and flexion moments of each HBM related to each THOR (absolute magnitudes). HBM peak loads from lumbar level with overall peak value, compression force and flexion moment considered separately. Most slope coefficients were significant (see Table B1).

Additionally, analyses in this study have extracted peak compression forces and flexion moments among all lumbar levels (T12-L5), with the assumption that the overall peaks represent the most injurious level. However, the overall peaks from most HBMs occurred at T12, L4 or L5. Thus, some of the peak loads extracted from the simulations were not from the range of anatomically equivalent lumbar levels (T12-L2) (Fig. B3). Supplementary analysis illustrated that the relationship between HBM and THOR peak loads was HBM measurement location dependent, primarily for flexion moments (Fig. 6 and 7). Peak compression forces at all HBM lumbar levels displayed positive relationships with THOR load cell compression forces, with the relationships consistently significant across lumbar levels for GHBMC, except at L5, and largely THOR-model-dependent and level-dependent for THUMS (Fig. 6; Table B1). The relationship of HBM and THOR flexion moments switched directionality at the mid-lumbar column, with positive trends at the thoracolumbar junction, negative trends near the pelvis, and mixed slope coefficient significance throughout (Fig. 7; Table B1).

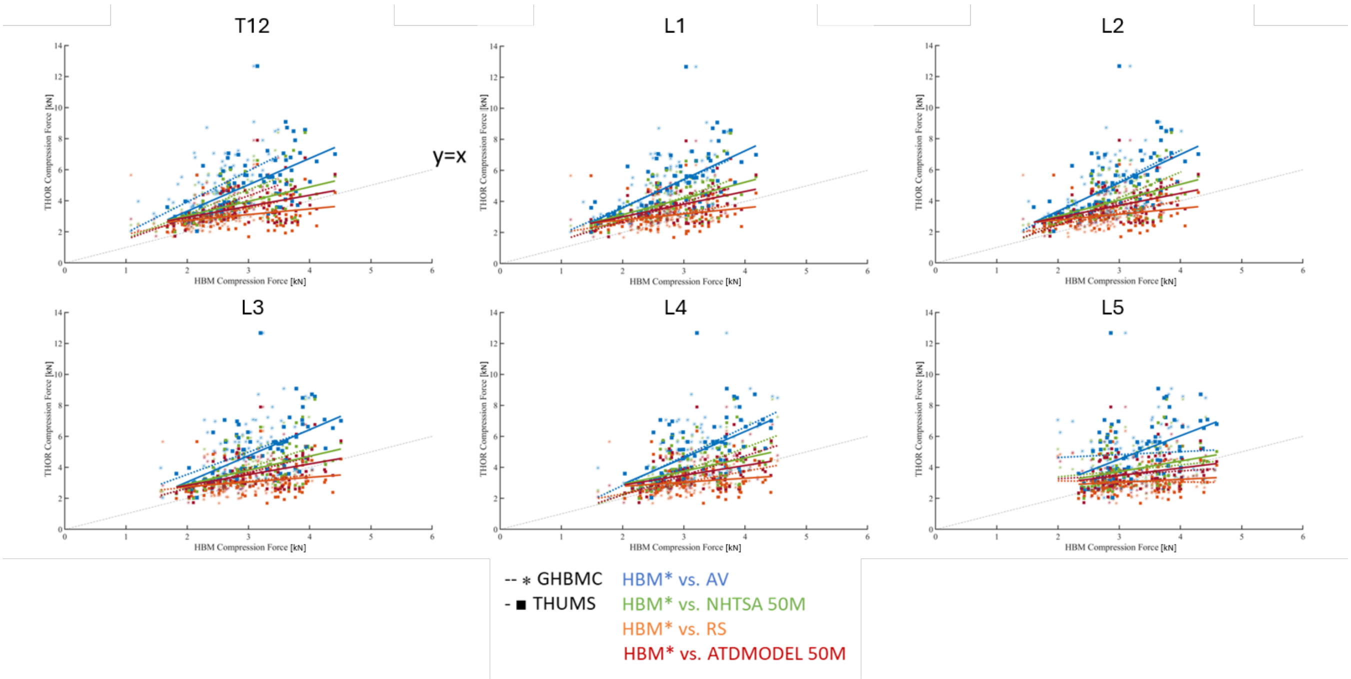

Fig. 6. Peak compression forces of each HBM related to THOR (absolute magnitudes), by HBM lumbar spine level. Most slope coefficients were significant (see Table B3).

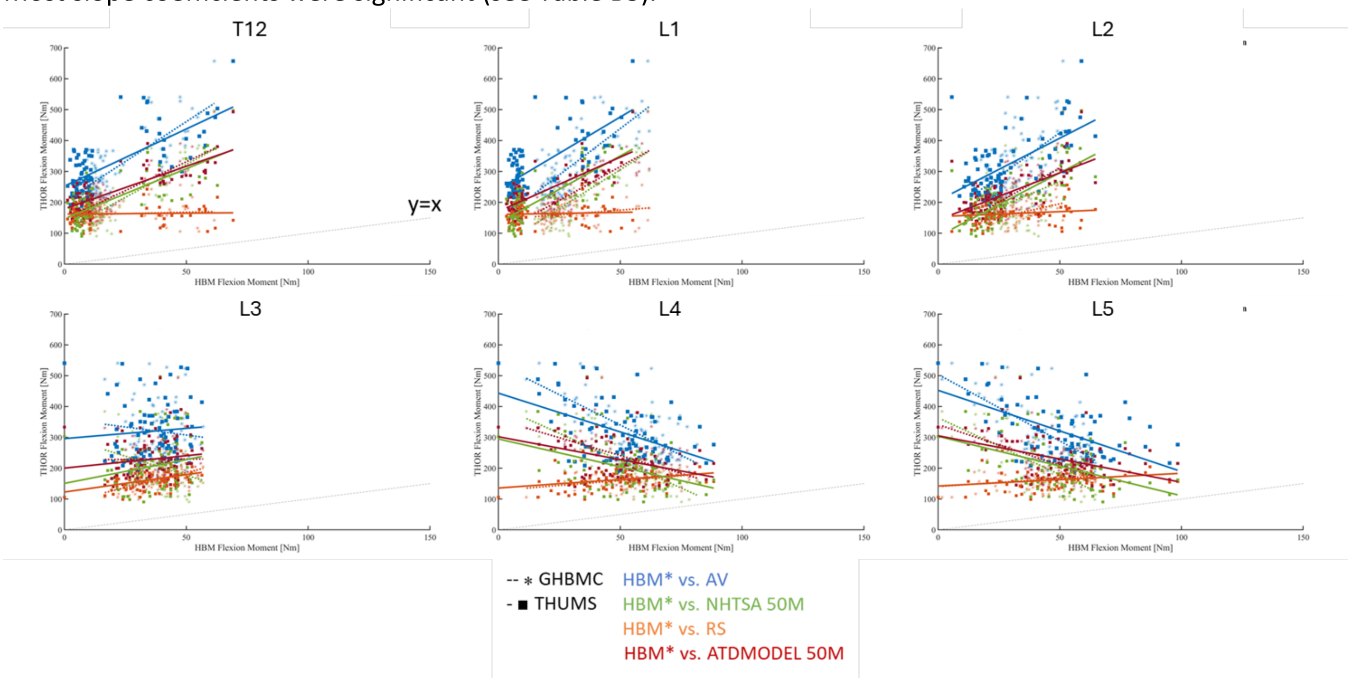

Fig. 7. Peak flexion moments of each HBM related to THOR (absolute magnitudes), by HBM lumbar spine level. Some slope coefficients were significant (see Table B3).

Peak probability of injury for GHBMC ranged from near 0% up to nearly 80% risk of injury (Fig. 8), with fairly dispersed data within the range. In general, the relationship between peak probability of lumbar spine injury as predicted by the GHBMC and each THOR model peak compression force and flexion moment were largely significantly positively related (Fig. 8.; Table B2). The highest risk for injury was generally measured in T12, and the risk decreased until L4 and L5 (Fig. 9 and 10). Further, the peak overall probability of injury from each simulation was measured in either T12 or L5 (Fig. B3). THOR peak compression forces were significantly related to GHBMC peak injury risk in all levels, except L5 (Fig. 9, Table B4). THOR peak flexion moments displayed varied relationships to GHBMC peak injury risk by level, with significantly positive relationships and relatively less variation (higher R^2) at the levels of the thoracolumbar junction, except for THOR-RS (Fig. 10, Table B4).

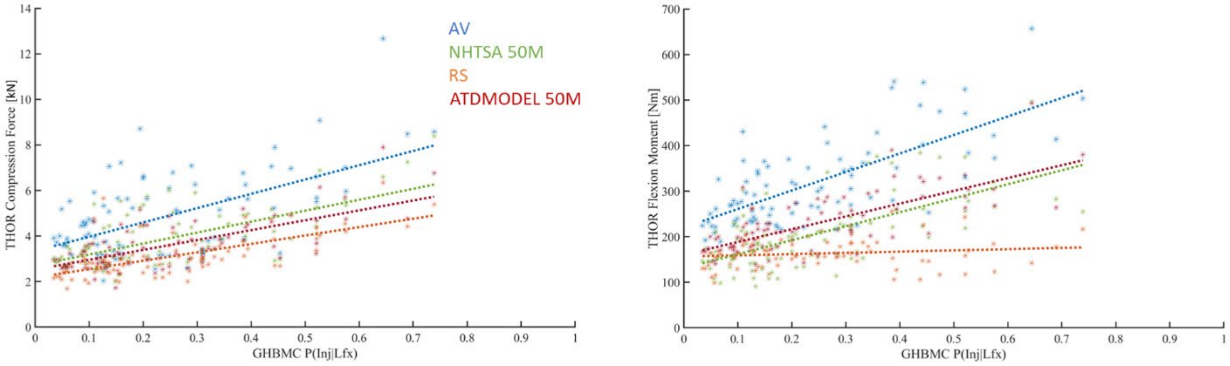

Fig. 8. Peak GHBMC probability of injury related to THOR compression forces and flexion moments (absolute magnitudes). Most slope coefficients were significant for compression force and flexion moment (see Table B2). GHBMC peak probability of injury from lumbar level with overall peak value.

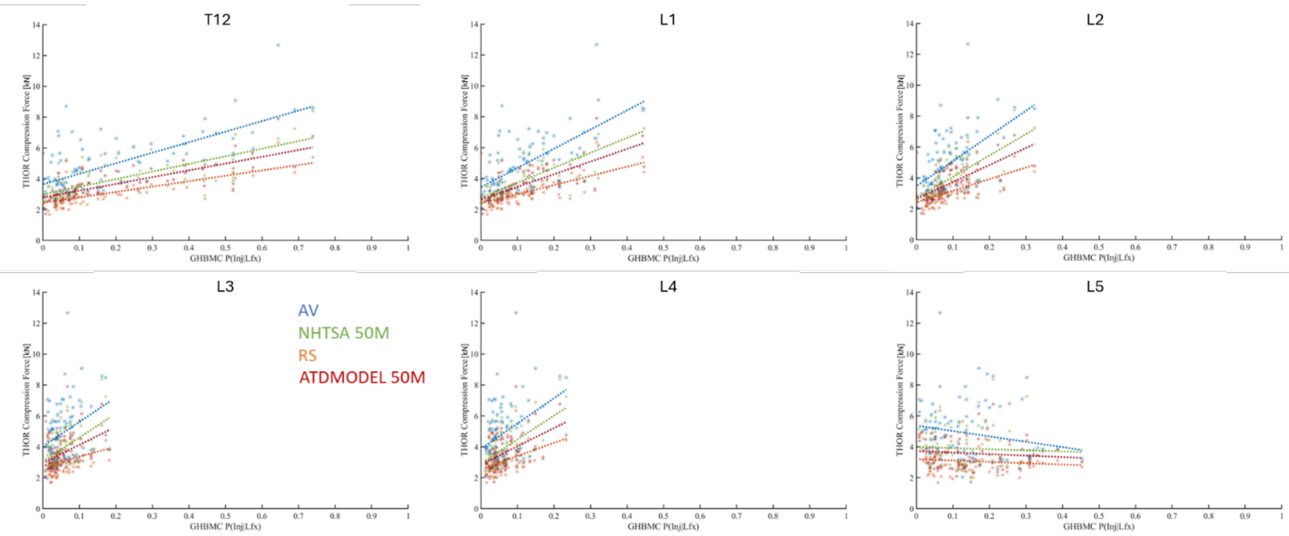

Fig. 9. Peak GHBMC probability of injury related to THOR compression forces (absolute magnitudes), by HBM lumbar spine level. All slope coefficients were significant, except for at L5 (see Table B4).

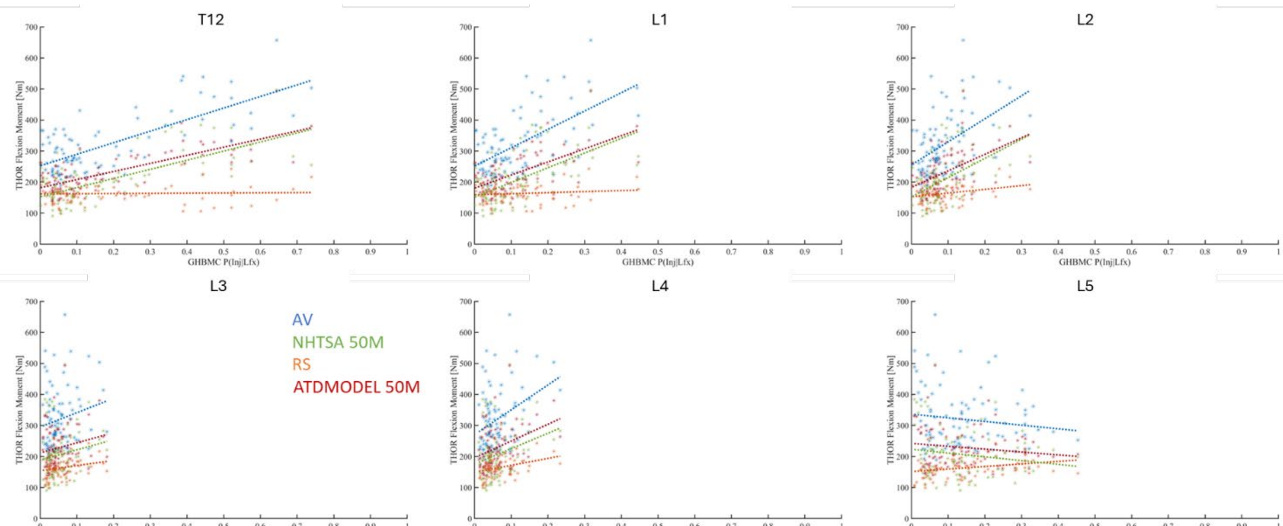

Fig. 10. Peak GHBMC probability of injury related to THOR flexion moments (absolute magnitudes), by HBM lumbar spine level. Some slope coefficients were significant (see Table B4).

IV. DISCUSSION

The cases analysed after accounting for premature termination and submarining were equally sampled at all factor levels, with the exception of fewer cases at larger torso angles and in vehicle seats. Thus, one limitation is that the final matched simulation cohort was compiled of a majority of upright and semi-rigid seat cases, which reflects the models' stabilities and tendencies to submarine. One of the primary outcomes of this study was the relationship between the peak lumbar spine compression force and flexion moment between each HBM and THOR across the matched non-submarining cases. In order to be able to create THOR injury criteria using a HBM, HBM loads should be positively correlated to THOR loads for the same changes in factors. In other words, it is expected that the primary lumbar spine loads of HBM and THOR in frontal crashes are equivalently sensitive to changes in relevant occupant and environment factors and respond in the same direction. When evaluating overall peak compression forces, all human surrogates displayed similar directionality, with higher HBM compression forces correlating to higher THOR compression forces. Many of the data were close to the y=x line with slope coefficients hovering around one, indicating a one-to-one relationship between HBM and THOR compression force on average. However, substantial variation in surrogate compression forces was observed, as evidenced by low R^2 values. The flexion moment relationship between each HBM and THOR displayed larger variation than compression forces, with mixed trends in peak flexion moments across the ten-parameter space and lumbar levels. The large variability within THOR flexion moments indicated highly sensitive behavior for each combination of factors. Overall, THOR-AV displayed the highest lumbar spine loads, and THOR-RS displayed the lowest lumbar spine loads, compared to both THOR-50M. Although no contact was established between the vehicle seatback and occupant in order to maintain initial postures, this was not believed to meaningfully affect lumbar spine loads since the occupants were exposed to solely frontal impact with limited simulated rebound. Therefore, the occupants would have experienced limited to no interaction with the seatback if a contact had been defined. Additionally, peak lumbar loads were the variables of interest, and those occurred around the time of peak pelvis and head forward excursion when the occupant's torso was the farthest distance from the seatback.

Additionally, lap belt and pelvis differences were identified between THOR and HBMs. THOR's pelvis flesh is stiffer and thicker than HBMs [40], which caused both physical THOR and virtual THOR to be seated higher and forward compared to HBMs and PMHS (aside from THOR-RS, for reasons described later in the paragraph) (Fig. 2). Further, the routed lap belt was positioned at a flatter sagittal angle for THOR and steeper sagittal angle for HBMs (Fig. B4). Additionally, the buttock and pelvis flesh of THOR is stiffer than that of the HBMs, which could have affected the interaction of the surrogate with the restraints and attenuation of loads transmitted up the spine. The THOR-RS was designed with less vertical buttock flesh to address the differences in vertical H-point locations between human surrogates and dummies [41–43]. Additionally, THOR-RS pelvis flesh has wider openings around the thigh "bones". This likely affects how the dummy interacts with the lap belt. However, the THOR-RS was largely insensitive to changes in the parameter space when directly related to the HBMs, and THOR-RS flexion moments saturated at approximately 200 Nm, compared to the other THOR models which measured peak flexion moments up to 700 Nm. This phenomenon was potentially due to the abdominal parts creating alternative load paths to offload the spine. Other changes in design between THOR-50M and other THOR variants exist, such as differences in the abdomen and pelvis geometry and material, and may influence the comparisons of resulting spine loads between THOR models. These models are commercially licensed, so UVA was generally not privy to specific differences in geometry and material.

The relationships between HBM and THOR peak loads were HBM measurement location dependent, primarily for flexion moments. Peak compression forces at all HBM lumbar levels displayed positive relationships with THOR load cell compression forces, except for few comparisons. The relationship of HBM and THOR flexion moments switched directionality at the mid-lumbar column, with positive trends at the thoracolumbar junction and negative trends near the pelvis. Further research is necessary to tease out the cause of the change in directionality, which could be influenced by occupant posture, seat characteristics, restraint engagement, and abdominal material properties, all of which were varied in this study. The anatomically equivalent HBM lumbar level for the THOR thoracic spine load cell is T12. T12 predicted among the highest GHBMC injury risks (Fig. B3), and the field data widely describes the thoracolumbar junction as the most frequently injured region [1–2], as well as PMHS in frontal impact sled environments sustained fractures at the thoracolumbar junction [3][4][6][8–9][12]. For future work, it is suggested that the loads at the anatomically equivalent location of T12 be solely considered when developing criteria for THOR since GHBMC injury risk and THOR force/moment comparisons were positively, monotonically related with less variation (higher R^2) than other comparisons. Additionally, THOR loads increased at a higher rate than HBMs, with slope coefficients greater than one. A limitation within the industry that infiltrated this study is that ATD lower spine responses (T12; thoracic spine load cell) are not controlled or critiqued against qualification tests. The resulting computational models are based on specific hardware, but it has not been verified if such hardware represents the dummy population, as there is no qualification requirement or standard. The introduction of any future dummy injury risk prediction tools, such as injury risk functions or injury assessment reference values, utilising thoracic spine load-cell data shall be preceded or accompanied by the introduction of controlled in dummy qualification for that load cell. If the load-cell data is not regularly compared to qualification requirements, then there is no guarantee that the hardware responses are stable.

Ultimately, vehicle regulation may involve both physical testing and virtual testing to optimise safety countermeasures and certify vehicles within allowable lumbar spine loading. While variable biofidelity of HBMs relative to humans can be accounted for when developing HBM-specific injury risk prediction [23][51], an inherent assumption, and potential limitation, is that virtual dummies adequately represent the physical dummy. Design of safety countermeasures using HBM as a link between humans and dummies also requires that the measurements from physical dummies are repeatable across dummies from the same and different manufacturers. These premises are critical when applying virtual ATD-specific injury risk prediction to its physical counterpart and must be checked. If virtual and physical dummy equivalence cannot be achieved or variation among physical dummies is deemed too large, then one or more possible courses of action are necessary: (1) improve virtual ATD biofidelity relative to its physical counterpart, (2) perform additional steps to correct for differences in virtual and physical ATD biofidelity and subsequent injury risk prediction tools, or (3) directly relate HBMs to physical ATDs to create ATD-specific injury risk prediction tools. Thus, further research is necessary before attempting to translate compression and flexion-based injury risk from GHBMC to THOR, such as determining factor-specific sensitivities within the 10-parameter simulation space. Advancements in countermeasure design have been beneficial in generally reducing injuries and fatalities. However, there is a delicate balance of optimising design when considering submarining, torso pitch, and alternative load paths across various occupant postures and vehicle environments.

V. CONCLUSION

This is the first study to systematically evaluate multiple THOR variants and HBMs regarding lumbar spine response under parameterised frontal impact conditions, establishing foundational relationships for translating HBM-based lumbar injury metrics derived from human data to ATDs and enabling the use of ATD lumbar load-cell data to assess occupant injury risk in future vehicles. Lumbar spine loads varied across surrogates due to differences in anatomy, construction, and instrumentation location. The Lfx injury metric in the GHBMC predicted the highest injury risk at the T12 vertebrae, consistent with PMHS and field data, aligning PMHS and ATD predictions with the anatomical location of the load cell. This alignment enables direct comparison of forces and moments between PMHS, HBMs, and ATDs. The study also enables future ATD injury assessment using PMHS-derived injury risk functions based on force and moment linked to an HBM, though moment evaluation requires further investigation due to its variability.

VI. ACKNOWLEDGEMENTS

The first set of simulations was funded by the National Highway Traffic Safety Administration (NHTSA). The second set of simulations was funded by Partnership for Dummy Technology and Biomechanics (PDB).

VII. REFERENCES

1. Pintar, F. A., Yoganandan, N., Maiman, D. J., Scarboro, M., Rudd, R. W. (2012) Thoracolumbar spine fractures in frontal impact crashes. *Annals of Advances in Automotive Medicine*, **56**: pp.277–283.
2. Shaikh, J., Thathia, H., Lubbe, N. (2020) Lumbar spine injuries in motor vehicle crashes. Proceedings of the International Research Council on the Biomechanics of Injury (IRCOBI Asia), 2020, Beijing, China.
3. Begeman, P. C., King, A. I., Prasad, P. (1973) Spinal loads resulting from –Gx acceleration. Proceedings of the Stapp Car Crash Conference, 1973, Coronado, CA.

4. Kallieris, D., Mattern, R., Schmidt, G., Warth, D. (1984) Kinematic and spinal column injuries in active and passive passenger protection: results of simulated frontal collisions. Proceedings of the International Research Council on the Biomechanics of Impact (IRCOBI), 1984, Delft, The Netherlands.
5. Patrick, L. M., Levine, R. S. (1975) Injury to unembalmed belted cadavers in simulated collisions. Proceedings of the Stapp Car Crash Conference, 1975, San Diego, CA, pp.79–115.
6. Richardson, R., Donlon, J. P., *et al.* (2020) Kinematic and injury response of reclined PMHS in frontal impacts. *Stapp Car Crash Journal*, **64**: pp.85–153.
7. Uriot, J., Potier, P., Baudrit, P., Trosseille, X., Richard, O., Douard, R. (2015) Comparison of HII, HIII and THOR dummy responses with respect to PMHS sled tests. Proceedings of the International Research Council on the Biomechanics of Injury (IRCOBI), 2015, Lyon, France, pp.435–451.
8. Rouhana, S. W., Bedewi, P. G., *et al.* (2003) Biomechanics of 4-point seat belt systems in frontal impacts. *Stapp Car Crash Journal*, **47**: pp.367–399.
9. Shin, J., Donlon, J. P., *et al.* (2023) Comparison of thoracolumbar spine kinematics and injuries in reclined frontal impact sled tests between mid-size adult female and male PMHS. *Accident Analysis & Prevention*, **193**: p.107334.
10. Baudrit, P., Uriot, J., Richard, O., Debray, M. (2023) Investigation of potential injury patterns and occupant kinematics in frontal impact with PMHS in reclined postures. *Stapp Car Crash Journal*, **66**(1).
11. Yoganandan, N., Somasundaram, K., Pintar, F. A. (2023) Analysis of experimental injuries to obese occupants with different postures in frontal impact. *Accident Analysis & Prevention*, **193**: p.107294.
12. Somasundaram, K., Humm, J. R., Yoganandan, N., Hauschild, H., Driesslein, K., Pintar, F. A. (2023) Obese occupant response in reclined and upright seated postures in frontal impacts. *Stapp Car Crash Journal*, **66**.
13. Somasundaram, K., Hauschild, H., Driesslein, K., Pintar, F. A. (2023) Small female occupant response in reclined and upright seated postures in frontal impacts. *Journal of Biomechanical Engineering*, **146**(3): p.031002.
14. Holdsworth, F. W. (1963) Fractures, dislocations, and fracture-dislocations of the spine. *Journal of Bone and Joint Surgery*, **45**(1): pp.1534–1551.
15. Roaf, R. (1960) A study of the mechanics of spinal injuries. *Journal of Bone and Joint Surgery*, **42**: pp.810–823.
16. Kifune, M., Panjabi, M. M., Arand, M., Liu, W. (1995) Fracture pattern and instability of thoracolumbar injuries. *European Spine Journal*, **4**(2): pp.98–103.
17. Adams, M. A., Dolan, P. (2011) Biomechanics of vertebral compression fractures and clinical application. *Archives of Orthopaedic and Trauma Surgery*, **131**: pp.1703–1710.
18. Mick, C. (1985) The management of trauma, pp.659–680. W.B. Saunders, Philadelphia, PA.
19. Kaufman, R. P., Ching, R. P., Willis, M. M., Mack, C. D., Gross, J. A., Bulger, E. M. (2013) Burst fractures of the lumbar spine in frontal crashes. *Accident Analysis & Prevention*, **59**: pp.153–163.
20. Wang, M. C., Pintar, F. A., Yoganandan, N., Maiman, D. J. (2009) The continued burden of spine fractures after motor vehicle crashes. *Journal of Neurosurgery: Spine*, **10**: pp.86–92.
21. Tushak, S. K., Donlon, J. P., *et al.* (2022) Failure tolerance of the human lumbar spine in combined compression and flexion loading. *Journal of Biomechanics*, **135**: p.111051.
22. Tushak, S. K., Gepner, B. D., Forman, J. L., Hallman, J. J., Pipkorn, B., Kerrigan, J. R. (2023) Human lumbar spine injury risk in dynamic combined compression and flexion loading. *Annals of Biomedical Engineering*, **51**: pp.1216–1225.
23. Tushak, S. K., Gepner, B. D., *et al.* (2023) Human body model lumbar spine fracture risk prediction. Proceedings of the International Research Council on the Biomechanics of Injury (IRCOBI), 2023, Cambridge, United Kingdom.
24. Huelke, D. F., Mackay, G. M., Morris, A. (1995) Vertebral column injuries and lap-shoulder belts. *Journal of Trauma*, **38**(4): pp.547–556.
25. Richards, D. M. S. P., Carhart, M. P., *et al.* (2006) Incidence of thoracic and lumbar spine injuries for restrained occupants in frontal collisions. *Annals of Advances in Automotive Medicine*, **50**: pp.119–133.
26. Miniaci, A., McLaren, A. C. (1989) Anterolateral compression fracture of the thoracolumbar spine – a seat belt injury. *Clinical Orthopaedics and Related Research*, **240**: pp.153–156.

27. Ejima, S., Kohoyda-Inglis, C., *et al.* (2018) Thoracolumbar spine fracture occurring in obese people involved in motor vehicle crashes. Proceedings of the International Research Council on the Biomechanics of Injury (IRCOBI), 2018, Athens, Greece.
28. Boyle, K. J., Reed, M. P., Zaseck, L. W., Hu, J. (2019) A human modelling study on occupant kinematics in highly reclined seats during frontal crashes. Proceedings of the International Research Council on the Biomechanics of Injury (IRCOBI), 2019, Florence, Italy.
29. Gepner, B. D., Draper, D., *et al.* (2019) Comparison of human body models in frontal crashes with reclined seatback. Proceedings of the International Research Council on the Biomechanics of Injury (IRCOBI), 2019, Florence, Italy.
30. Grébonval, C., Trosseille, X., Petit, P., Wang, X., Beillas, P. (2021) Effects of seat pan and pelvis angles on the occupant response in a reclined position during a frontal crash. *PLOS ONE*, **16**(9): e0257292.
31. Jones, D. A., Gaewsky, J. P., *et al.* (2016) Lumbar vertebrae fracture injury risk in finite element reconstruction of CIREN and NASS frontal motor vehicle crashes. *Traffic Injury Prevention*, **17**(Suppl.1): pp.109–115.
32. Rawska, K., Gepner, B. D., *et al.* (2019) Submarining sensitivity across varied anthropometry in an autonomous driving system environment. *Traffic Injury Prevention*, **20**(sup2): pp.S123–S127.
33. Katsuhara, T., Takahira, Y., Hayashi, S., Kitagawa, Y., Yasuki, T. (2017) Analysis of driver kinematics and lower thoracic spine injury in world endurance championship race cars during frontal impacts. *SAE International Journal of Transportation Safety*, **5**(1): pp.120–132.
34. Tang, L., Zheng, J., Hu, J. (2020) A numerical investigation of factors affecting lumbar spine injuries in frontal crashes. *Accident Analysis & Prevention*, **136**: p.105400.
35. Amenson, T. T., Begeman, P. C., Melvin, J. W., Grimm, M. J. (2008) Development of the MADYMO race car driver model for frontal impact simulation and thoracolumbar spine injury prediction. *SAE International Journal of Passenger Cars – Electronic and Electrical Systems*, **1**(1): pp.630–651.
36. Uriot, J., Potier, P., Baudrit, P., Trosseille, X., Richard, O., Douard, R. (2015) Comparison of HII, HIII and THOR dummy responses with respect to PMHS sled tests. Proceedings of the International Research Council on the Biomechanics of Injury (IRCOBI), 2015, Lyon, France.
37. Richardson, R., Jayathirtha, M., *et al.* (2020) Thoracolumbar spine kinematics and injuries in frontal impacts with reclined occupants. *Traffic Injury Prevention*, **21**(sup): pp.S66–S71.
38. Mroz, K., Östling, M., *et al.* (2020) Effect of seat and seat belt characteristics on lumbar spine and pelvis loading of the SAFER human body model in reclined postures. Proceedings of the International Research Council on the Biomechanics of Injury (IRCOBI), 2020, Online.
39. Gepner, B. D., Perez-Rapela, D., *et al.* (2022) Evaluation of GHBMC, THUMS and SAFER human body models in frontal impacts in reclined postures. Proceedings of the International Research Council on the Biomechanics of Injury (IRCOBI), 2022, Porto, Portugal.
40. Shin, J., Donlon, J. P., *et al.* (2022) Biofidelity evaluation of the Hybrid-III 50th male and the THOR-50M in reclined frontal impact sled tests. Proceedings of the International Research Council on the Biomechanics of Impact (IRCOBI), 2022, Cambridge, United Kingdom.
41. Donlon, J. P., Forman, J., Gepner, B., Kerrigan, J. R. (2023) Continuing refinement of THOR for reclined postures – testing to evaluate prototype pelvis modifications. University of Virginia Center for Applied Biomechanics report, Charlottesville, VA.
42. Forman, J., Kerrigan, J., *et al.* (2023) THOR-50M for reclined seating: positioning assessment. National Highway Traffic Safety Administration report.
43. Dyer, M., Marshall, W., Forman, J. (2023) THOR-50M modifications for reclined seating design change report (phases 1 & 2). National Highway Traffic Safety Administration report.
44. Richardson, R. E., Gepner, B., Kerrigan, J. R., Forman, J. L. (2024) Evaluation of lap belt–pelvis load transfer in frontal impact simulations using finite element occupant models. *Traffic Injury Prevention*, **25**(8): pp.1137–1145.
45. Montgomery, D. C. (2017) *Design and analysis of experiments*, 8th ed. John Wiley & Sons, New York, NY.
46. ENOP sled environment models, www.gitlab.com/piper-project.org [14 Apr 2026].
47. Toyota Auris vehicle seat model, www.openvt.eu [14 Apr 2026].

48. Reed, M. P., Ebert, S. M., Jones, M. L. (2019) Posture and belt fit in reclined passenger seats. *Traffic Injury Prevention*, **20**(sup1): pp.S38–S42.
49. Louden, A. (2019) Revised THOR 50th percentile male dummy seating procedure. National Highway Traffic Safety Administration report, Washington, DC.
50. Tushak, S. K., Gepner, B. D., *et al.* (2022) Evaluation of the GHBMC lumbar spine in sub-injurious and injurious loading. Proceedings of the International Research Council on the Biomechanics of Injury (IRCOBI), 2022, Porto, Portugal.
51. Forman, J., Kulkarni, S., *et al.* (2022) A method for thoracic injury risk function development for human body models. Proceedings of the International Research Council on the Biomechanics of Injury (IRCOBI), 2022, Porto, Portugal.

[1] **APPENDIX A: Further Description of Methods**

Sampling and Parameterisation

A full-factorial simulation study was not feasible, as it would have required 3,072 simulations. Thus, sub-sampling reduced the number to 192 sled-style frontal impact simulations per surrogate (Eq. A1). A sixteenth fractional factorial design with a resolution of IV was introduced for the eight variables sampled at two levels, resulting in 16 runs [45]. The resulting sampling scheme pre-allocated combinations of factor levels such that each factor was equally sampled and information of the entire parameter space was gained via Design of Experiments (Table A1). The sixteenth fractional-factorial was applied within each combination of torso angle (three levels) and restraint type (categorical, four levels).

$$\#\,Simulations = (2^{8-4} Runs) * (3\ Torso\ Angles) * (4\ Restraint\ Types) \qquad \text{(Eq. A1)}$$

TABLE A1
Combinations of factors for the sixteenth fractional factorial design for this study's eight variables with two levels. The order of factors (#s 1-8) was determined randomly.

Run #	1. Shoulder Belt Takeoff Angle	2. Organ Stiffness	3. Flesh Stiffness	4. Delta V	5. Seat Type	6. Pelvis-Spine Orientation	7. Knee Bolster	8. Lap Belt Anchor Position
1	Negative	Nominal	Nominal	40	Semi-Rigid	Nominal	Off	Nominal
2	Positive	Nominal	Nominal	40	Semi-Rigid	Posterior	On	Forward
3	Negative	5x	Nominal	40	Vehicle	Nominal	On	Forward
4	Positive	5x	Nominal	40	Vehicle	Posterior	Off	Nominal
5	Negative	Nominal	5x	40	Vehicle	Posterior	On	Nominal
6	Positive	Nominal	5x	40	Vehicle	Nominal	Off	Forward
7	Negative	5x	5x	40	Semi-Rigid	Posterior	Off	Forward
8	Positive	5x	5x	40	Semi-Rigid	Nominal	On	Nominal
9	Negative	Nominal	Nominal	51	Vehicle	Posterior	Off	Forward
10	Positive	Nominal	Nominal	51	Vehicle	Nominal	On	Nominal
11	Negative	5x	Nominal	51	Semi-Rigid	Posterior	On	Nominal
12	Positive	5x	Nominal	51	Semi-Rigid	Nominal	Off	Forward
13	Negative	Nominal	5x	51	Semi-Rigid	Nominal	On	Forward
14	Positive	Nominal	5x	51	Semi-Rigid	Posterior	Off	Nominal
15	Negative	5x	5x	51	Vehicle	Nominal	Off	Nominal
16	Positive	5x	5x	51	Vehicle	Posterior	On	Forward

Delta-V

Delta-v was varied at 40 km/h and 51 km/h, with the latter level used extensively in the literature to study reclined occupants [6][9][36], and the former level being scaled from 51 km/h (Fig. A1).

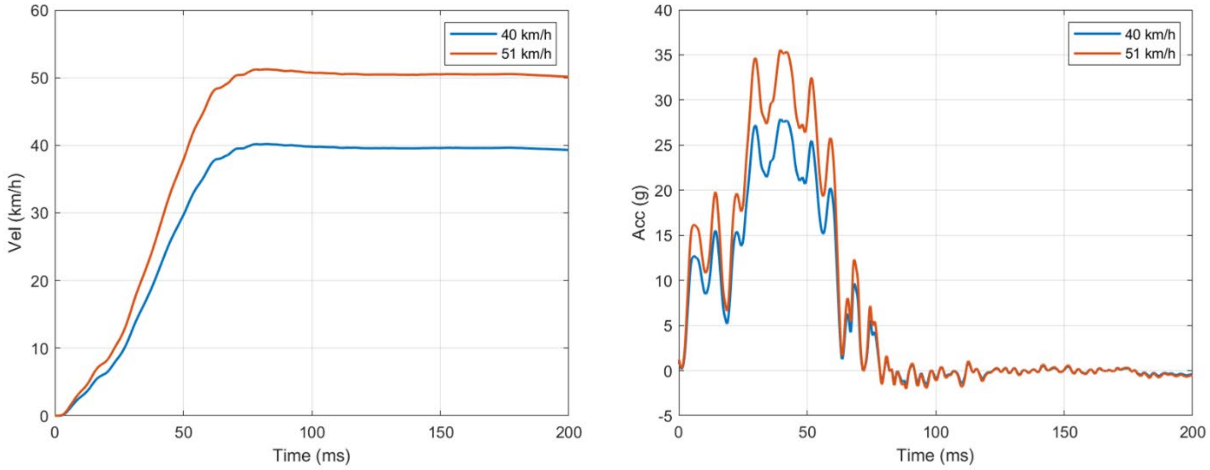

Fig. A1 Impact pulses utilised in the simulation study, depicted in delta-velocity (left) and acceleration (right).

Restraint Modifications and Integration with Seats

Restraint type was a categorical variable with stepwise changes in one aspect of the restraint (load limiters or pretensioner) from the baseline model. The baseline model (Restraint 1) included triple pretensioning (buckle at 3 ms, outboard anchor at 10 ms, and shoulder belt retractor at 10 ms) and shoulder belt load limiting of 3.5 kN [6][9][29][39–40]. Subsequent levels included reducing the shoulder belt load limiter to 2.5 kN (Restraint 2), replacing the lap belt functionality to include lap belt load limiters of 5 kN (outboard anchor) and 7 kN (buckle) (Restraint 3), as they have been suggested to reduce lumbar spine loads [39][40], and replacement of the outboard anchor pretensioner to a static anchor (Restraint 4), resulting in a dual pretensioner system similar to more traditional belt systems in modern vehicles.

The changes were implemented via restraint parameters (see Table A2). The second level reflected a reduction in shoulder belt load limiting to 2.5 kN and was achieved by changing the parameters for the initial force in the shoulder belt load limiter from 2.7 to 1.7 kN, as well as the second value in the load limiting curve from 2.5 to 1.5 kN (Table A2). The third restraint type level included lap belt load limiters on both the buckle and outboard anchor, which required both model parameters to be switched from 50 kN to 7 and 5 kN, respectively (Table A2). The fourth restraint type turned off the outboard anchor pretensioner to represent a dual-pretensioner system (Table A2). This was achieved by changing the slipring function to be "locked" from the start of the simulation.

TABLE A2
Modifications of the generic restraint model necessary to achieve each restraint type.

Restraint Type	Parameter Needing to Be Changed	Baseline Value	New Restraint Value
Restraint 1: Baseline	None		
Restraint 2	R1LL1fo	2.7	1.7
	Load Curve #500603 Ordinate Pt. 2	2.5	1.5
Restraint 3	BuLL1fo	50.0	7.0
	EBLL1fo	50.0	5.0
Restraint 4	EBlock	10000.0	0.01
	Slipring Element #40000005 LTIME	0.0	"EBlock"

These changes were verified in re-runs of the validation case for all restraint modifications to confirm appropriate functionality of the restraints (Fig. A2 and A3). Specifically, Restraint 2 displayed shoulder belt load limiting initiating at 1.7 kN and increasing to approximately 2.5 kN (Fig. A2), with a corresponding increase in shoulder belt displacement (Fig. A3). Restraint 3 displayed the appropriate loading limiting in both the outboard lap belt and buckle (Fig. A2), which was reflected in both displacement measurements (Fig. A3). Restraint 4 displayed no outboard lap belt payout (10 mm readout due to belt stretch or method of measurement) (Fig. A3), which ultimately affected initial lap belt forces but not peak lap belt forces (Fig. A2).

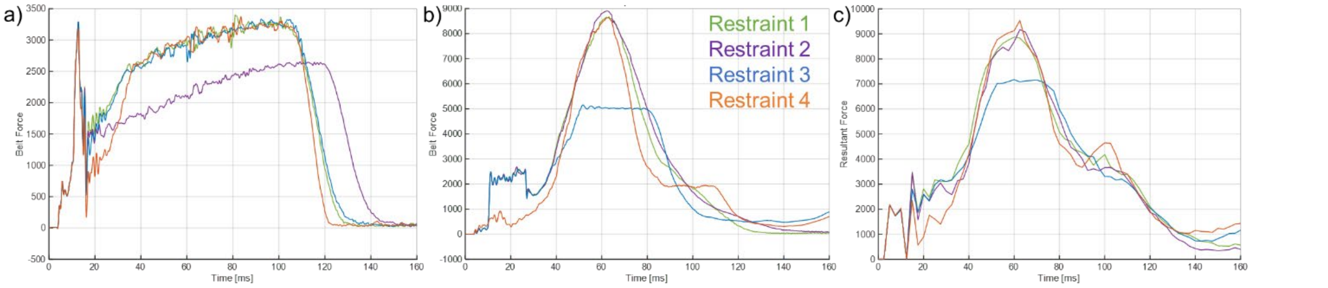

Fig. A2. Belt forces for the (a) shoulder belt, (b) outboard lap belt, and (c) inboard buckle with all restraint types.

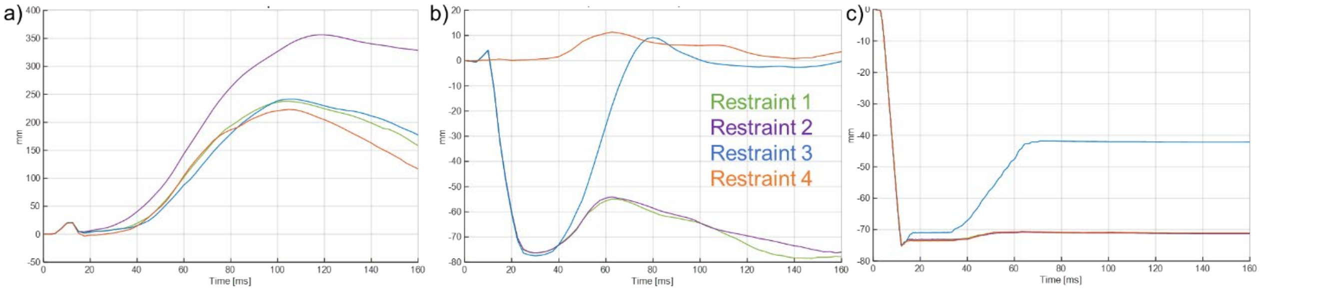

Fig. A3. Belt displacements for the (a) shoulder belt, (b) outboard lap belt, and (c) inboard buckle with all restraint types.

Additionally, the nominal lap belt anchorage positions matched those of previous sled tests and simulations with this environment at approximately 63° from the H-point to the anchorage [6][9][29][39–40], and the forward position was located 52 mm forward which dictated the upper limit of the FMVSS lap belt corridor of 75°(Fig. A). The forward position was obtained by a +52 mm rigid body translation of the inboard and outboard lap belt anchors. The lap belt anchors were not moved vertically or laterally from the nominal position to remain consistent. As a result, the anchor structures penetrated the structure of the Vehicle seat pan. Since no contact was defined, this did not affect the functionality of the restraint from as it was intended.

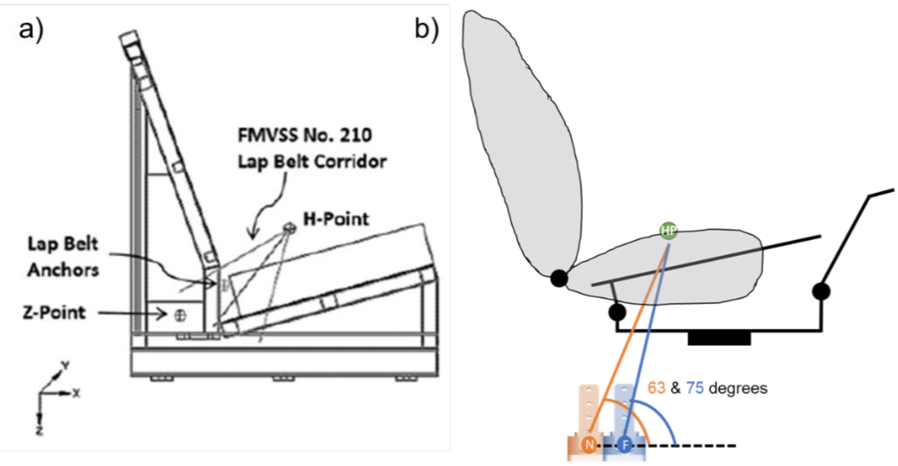

Fig. A (a) FMVSS No. 210 lap belt corridor measurements and (b) corresponding measurements for the current study's anchorages and seats.

Shoulder belt take-off angle was varied to be positive or negative, with specific values selected as +12° [6][9][29][39–40] and the y-axis mirrored value of -12°, achieved by rigidly translating the D-ring and B-pillar vertically. The D-ring positions to obtain +/- 12°shoulder belt take-off angles were specific to each posture and seat variation of each surrogate. The appropriate vertical translations were determined as the necessary translations from the stock position to achieve +/-12°angles between the shoulder and D-ring. Subsequently, the D-ring and B-pillar structure was rigidly translated vertically to the appropriate position but not adjusted for-aft or laterally.

Two seat models were included. The semi-rigid seat model, designed to mimic the stiffness of vehicle seats [36], was tuned to replicate functionality of previous reclined occupant sled tests and simulations [6][9][29][39–40] with the deformable seat pan angled at 15° and anti-submarining ramp angled at 30° from the horizontal.

Additionally, a publicly available 2010-2012 Toyota Auris vehicle seat model was included (25° seatback, mid-height headrest location, approximately 13° seat pan angle) [47]. Nominal anchorage positions for the semi-rigid seat were based on physical test boundary conditions [6][9]. H-point design specifications of both seats were used to equate restraint anchor positions between the native semi-rigid seat and vehicle seat with respect to the rotational axes of both seats, so that the relative position of the belt anchorages to the design H-point was the same with both seat models (Fig. A).

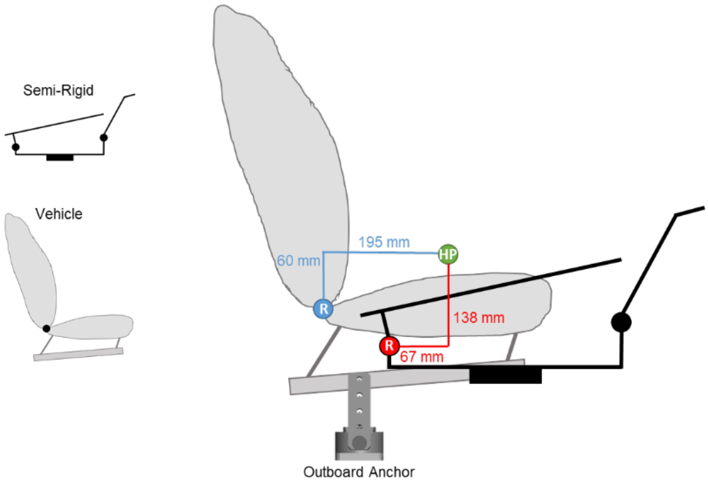

Fig. A. Definitions of the design H-point (HP) location to the rotational (R) seat axis for the semi-rigid and the vehicle seats that were used to place the nominal anchorage position.

Abdominal Cross-Sections and Scaling of Soft Tissue Material Properties

These cross-sections were defined to evaluate the effects of flesh and organ stiffness factors by comparing the forces borne by the soft tissues and bone for nominal and scaled soft tissues. Three separate abdominal cross-sections were defined at the L3 planar level: the first including skin, muscle, and adipose entities (name simplified to "flesh"), the second including bone and ligaments (name simplified to "bone"), and the last including abdominal organs and enclosing peritoneal lining (name simplified to "organs"). The identification of entities to include in the three abdominal cross-sections was performed as follows. First, a plane was defined across the abdomen and was aligned with the sagittal mid-plane of the L3 vertebra, perpendicular to the endplates (Fig. A3). All nodes and elements intersecting that plane were identified and automatically separated into three sets associated with the three abdominal cross-sections.

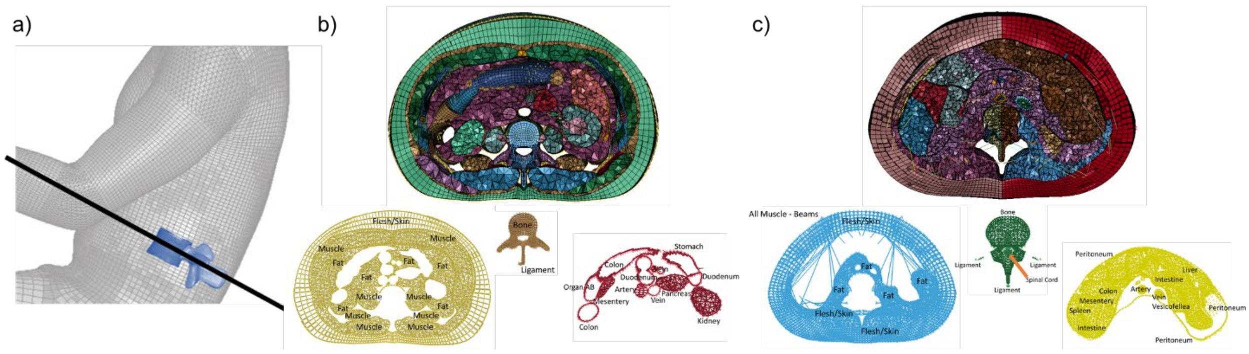

Fig. A3. Abdominal cross-section definition from (a) the planar L3 level for (b) GHBMC and (c) THUMS for the entities representing flesh, bone, and organs.

A similar approach was performed for THOR 50M-UVA-NHTSA, but abdominal cross-sections of anatomical equivalents were defined as: the jacket ("flesh"), spine load cell ("bone"), and abdominal foam ("organs"). A plane was defined across the abdomen and was aligned near the L3 anatomical equivalent [40] through the model's spine load cell beam element, perpendicular to the geometrical load cell (Fig. A4). Again, all nodes and elements intersecting that plane were identified and automatically separated into three sets associated with the three abdominal cross-sections.

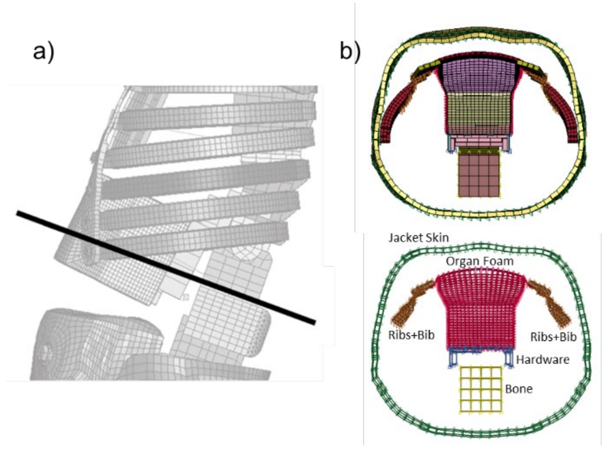

Fig. A4. THOR 50M-UVA-NHTSA abdominal cross-section definition from (a) the planar L3 level for (b) the entities representing flesh, bone, and organs.

The soft tissues identified for the abdominal cross-sections were scaled to represent an overall increase in abdominal stiffness compared to the nominal values of the surrogates. The overall effect of scaling abdominal stiffness was measured by comparing responses of abdominal impact tests (GHBMC: Hardy, 2001; THUMS: Cavanaugh et al., 1986; THOR: Abdomen Qualification Test). Each surrogate's abdominal impact environment was included as part of the surrogate download and was not created by the authors. The HBMs environments including the relevant surrogate represented PMHS tests with either a 48 kg (Hardy *et al*., 2001) or 32 kg (Cavanaugh *et al*., 1986) cylindrical bar impacting L3 at approximately 6 m/s. The THOR environment represented the 32 kg piston impacting the abdomen at 3.3 m/s. Each soft tissue stiffness was scaled by five times to ensure large enough difference in response (Fig. A5). Specifically, the scale factor was applied to either the load curve ordinates, elastic modulus, bulk modulus, or shear modulus depending on the material being scaled.

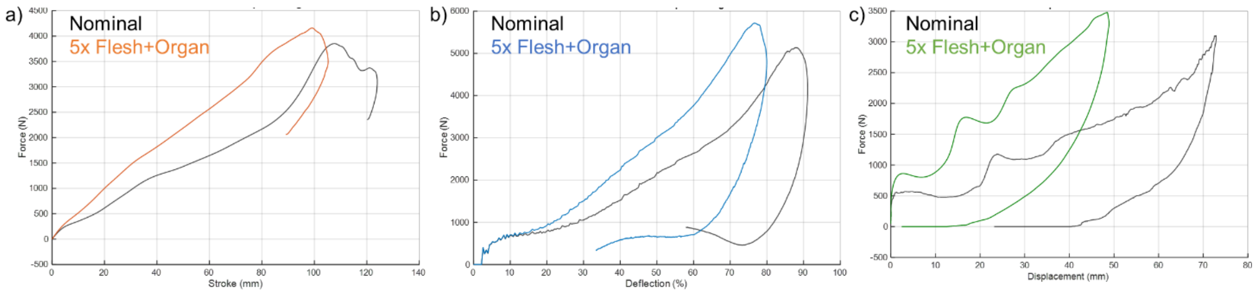

Fig. A5. Force-displacement response of (a) THUMS, (b) GHBMC, and (c) THOR 50M-UVA-NHTSA from the rigid bar abdominal impact before and after scaling the soft tissues.

Relatedly, the THOR 50M-UVA-NHTSA has been shown (internally in UVA-CAB) to exhibit contacting between two adjacent abdominal plates in the baseline recline case, typically resulting in early termination of the simulation. To prolong simulation duration, a pseudo contact with 5 mm thickness was defined between these two plates and utilised in all simulations with THOR 50M-UVA-NHTSA. The contact force between these plates was monitored to identify the range of this issue across the parameter space. In the second set of simulations with THOR 50M-ATDMODELS, RS, and AV, the flesh and organ stiffness for the THOR analog were not varied, and only nominal/stock values were utilised. Firstly, these two parameters were found not to substantially influence lumbar spine loads in the first set of simulations with the HBMs and THOR 50M-UVA-NHTSA. Additionally, and importantly, the material characteristics of these dummy parts were not able to be modified in the commercial models being used in this study.

VIII. APPENDIX B: ADDITIONAL RESULTS AND DISCUSSION

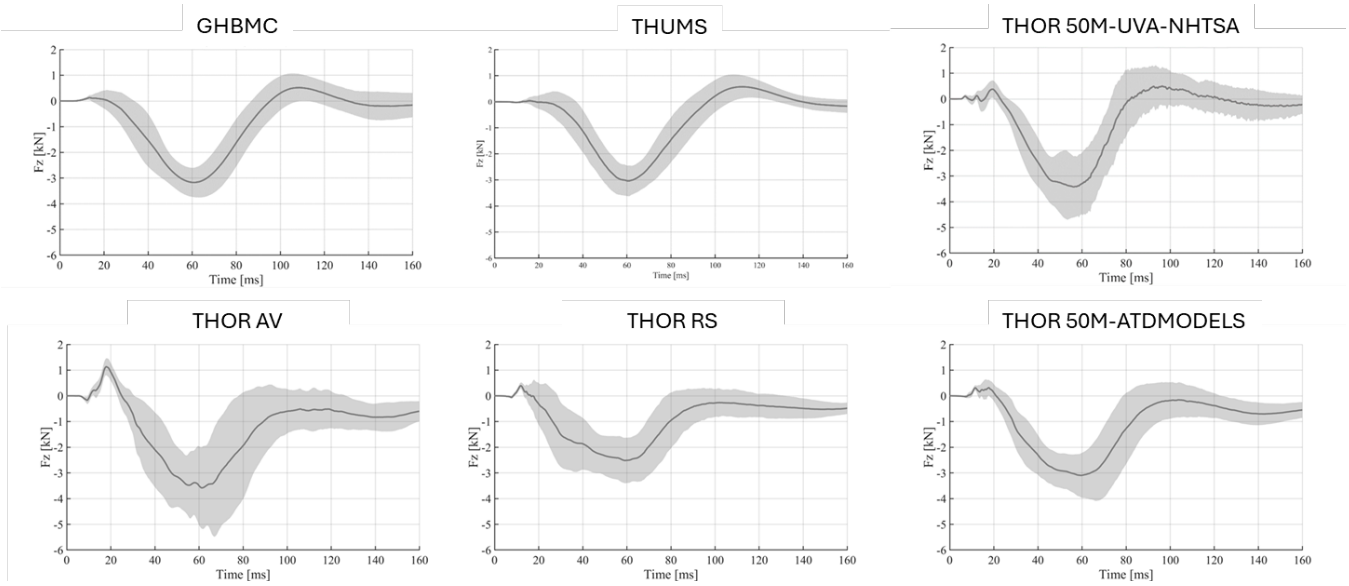

Fig. B1. Axial force of the lumbar level which experienced the highest peak compression force (one curve per surrogate simulation). Average (black line) and one standard deviation (grey shading) calculated at each time step.

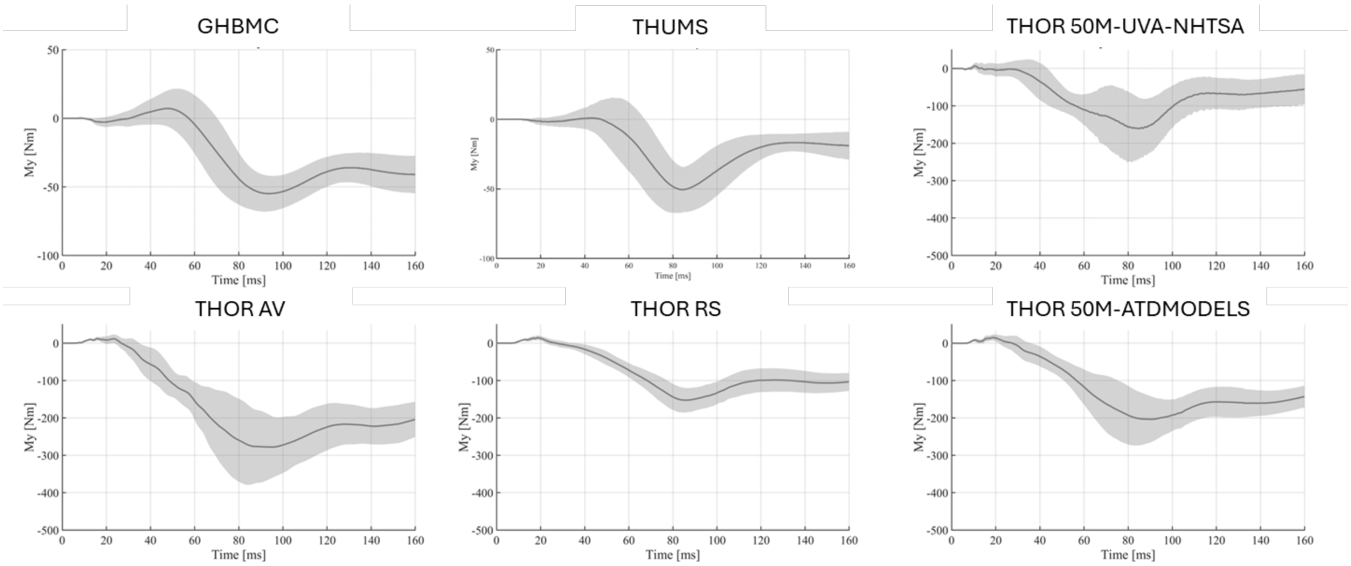

Fig. B2. Forward bending moment of the lumbar level which experienced the highest peak forward bending moment (one curve per surrogate simulation). Average (black line) and one standard deviation (grey shading) calculated at each time step.

TABLE B1
Statistical outcomes for each HBM-THOR peak load relationship.

		GHBMC vs. Y				THUMS vs. Y			
		50M-UVA-NHTSA	50M-ATDMODEL	AV	RS	50M-UVA-NHTSA	50M-ATDMODEL	AV	RS
Flexion Moment	Intercept	350.209	311.768	493.538	102.266	224.809	237.243	373.931	128.192
	Slope	-2.460	-1.411	-2.967	1.038	-0.332	-0.144	-0.960	0.617
	Slope p-value	0.004	0.046	0.004	0.003	0.613	0.789	0.226	0.020
	Adjusted R^2	0.036	0.036	0.085	0.092	-0.009	-0.011	0.006	0.053
Compression Force	Intercept	0.834	0.536	1.367	1.597	1.150	1.544	-0.723	2.105
	Slope	0.808	0.984	1.031	0.436	0.837	0.625	1.714	0.299
	Slope p-value	<<0.001	<<0.001	0.012	0.031	<<0.001	0.001	<<0.001	0.086
	Adjusted R^2	0.134	0.144	0.064	0.044	0.141	0.106	0.273	0.024

TABLE B2
Statistical outcomes for each GHBMC injury risk and THOR peak load relationship.

		GHBMC Pinj(Lfx) vs. Y			
		50M-UVA- NHTSA	50M-ATDMODEL	AV	RS
Flexion Moment	Intercept	130.825	160.274	220.158	156.391
	Slope	307.140	280.923	406.326	27.219
	Slope p-value	<<0.001	<<0.001	<<0.001	0.205
	Adjusted R^2	0.412	0.516	0.491	0.008
Compression Force	Intercept	2.708	2.523	3.340	2.177
	Slope	4.808	4.339	6.280	3.692
	Slope p-value	<<0.001	<<0.001	<<0.001	<<0.001
	Adjusted R^2	0.408	0.462	0.306	0.443

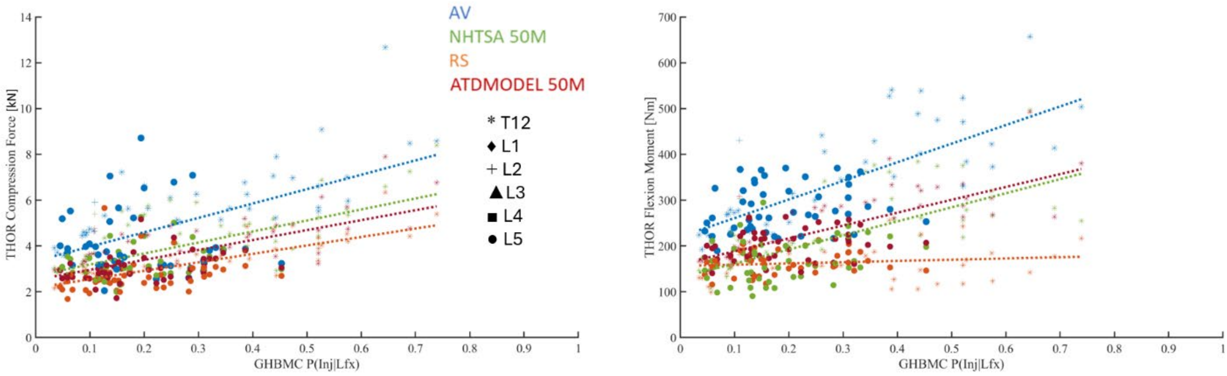

Fig. B3. Peak GHBMC probability of injury related to THOR compression forces and flexion moments (absolute magnitudes), with marker type indicating lumbar level with the highest value. Most slope coefficients were significant for compression force and flexion moment (see Table B2). GHBMC peak probability of injury from lumbar level with overall peak value.

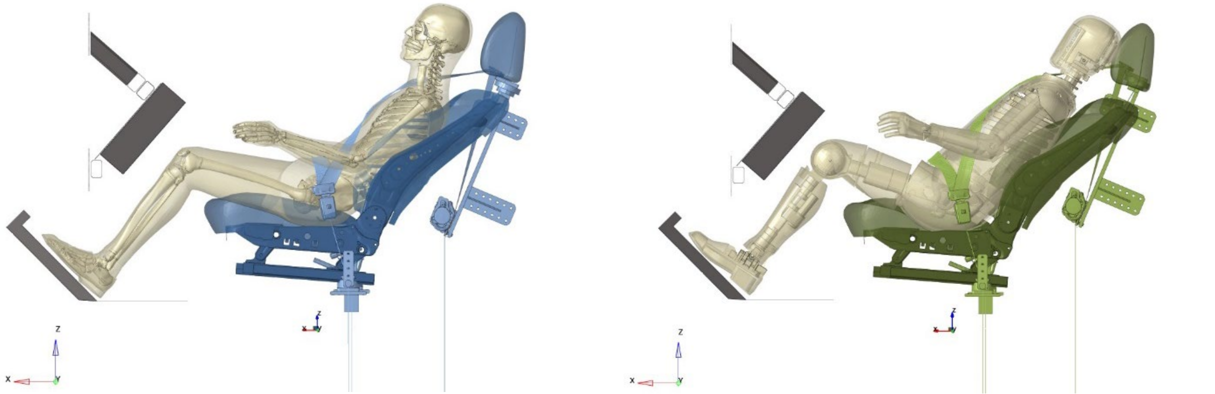

Fig. B4. Example case depicting the initial position of a matched GHBMC (left) and THOR-50M (right).

TABLE B3

Statistical outcomes for each HBM-THOR peak load relationship, by lumbar level.

			GHBMC vs. Y				THUMS vs. Y			
			50M-UVA-NHTSA	50M-ATDMODEL	AV	RS	50M-UVA-NHTSA	50M-ATDMODEL	AV	RS
T12	Flexion Moment	Intercept	109.869	144.876	203.089	158.861	147.296	178.930	252.431	161.937
		Slope	4.255	3.725	5.157	0.186	3.230	2.757	3.697	0.062
		p-value	<<0.001	<<0.001	<<0.001	0.445	<<0.001	<<0.001	<<0.001	0.745
		Adjusted R^2	0.625	0.715	0.622	-0.005	0.595	0.647	0.527	-0.011
	Compression Force	Intercept	0.002	0.102	-0.068	0.985	1.192	1.519	-0.072	2.017
		Slope	1.568	1.406	1.997	0.846	0.925	0.710	1.701	0.366
		p-value	<<0.001	<<0.001	<<0.001	<<0.001	<<0.001	<<0.001	<<0.001	0.016
		Adjusted R^2	0.368	0.412	0.262	0.191	0.231	0.187	0.353	0.058
L1	Flexion Moment	Intercept	54.590	97.329	138.930	144.932	134.154	170.607	241.652	160.810
		Slope	5.021	4.367	5.992	0.601	4.320	3.513	4.688	0.135
		p-value	<<0.001	<<0.001	<<0.001	0.037	<<0.001	<<0.001	<<0.001	0.583
		Adjusted R^2	0.606	0.685	0.585	0.040	0.628	0.619	0.499	-0.008
	Compression Force	Intercept	0.064	0.283	0.168	1.358	1.060	1.382	-0.084	2.025
		Slope	1.409	1.218	1.737	0.636	1.045	0.815	1.835	0.390
		p-value	<<0.001	<<0.001	<<0.001	0.001	<<0.001	<<0.001	<<0.001	0.008
		Adjusted R^2	0.331	0.343	0.219	0.116	0.314	0.263	0.435	0.072
L2	Flexion Moment	Intercept	103.440	90.950	141.373	108.824	90.157	142.703	205.742	154.035
		Slope	3.266	4.396	5.675	1.726	4.104	3.059	4.035	0.319
		p-value	0.001	<<0.001	<<0.001	<<0.001	<<0.001	<<0.001	<<0.001	0.187
		Adjusted R^2	0.112	0.324	0.243	0.195	0.580	0.478	0.376	0.009
	Compression Force	Intercept	-0.772	-0.345	-0.746	0.842	0.974	1.371	-0.325	2.020
		Slope	1.655	1.397	1.998	0.795	1.023	0.778	1.827	0.373
		p-value	<<0.001	<<0.001	<<0.001	<<0.001	<<0.001	<<0.001	<<0.001	0.015
		Adjusted R^2	0.376	0.371	0.239	0.153	0.279	0.222	0.401	0.059
L3	Flexion Moment	Intercept	300.606	227.330	359.682	88.210	150.797	200.349	295.979	122.655
		Slope	-2.467	0.046	-1.043	1.954	1.544	0.803	0.663	1.128
		p-value	0.017	0.957	0.413	<<0.001	0.062	0.239	0.513	0.001
		Adjusted R^2	0.056	-0.012	-0.004	0.243	0.030	0.005	-0.007	0.123
	Compression Force	Intercept	0.167	0.601	0.660	1.932	1.091	1.463	-0.330	2.166

		Slope	1.269	1.019	1.439	0.392	0.907	0.689	1.691	0.297
		p-value	<<0.001	<<0.001	<<0.001	0.056	<<0.001	<<0.001	<<0.001	0.048
		Adjusted R^2	0.271	0.246	0.031	0.052	0.228	0.180	0.359	0.035
L4	Flexion Moment	Intercept	401.934	356.815	536.753	128.157	294.903	302.005	443.412	135.790
		Slope	-3.549	-2.314	-3.932	0.632	-1.805	-1.481	-2.513	0.554
		p-value	<<0.001	<<0.001	<<0.001	0.009	<<0.001	<<0.001	<<0.001	0.010
		Adjusted R^2	0.413	0.257	0.341	0.068	0.130	0.131	0.175	0.068
	Compression Force	Intercept	-0.769	-0.303	-0.940	0.836	1.200	1.594	-0.502	2.269
		Slope	1.507	1.259	1.884	0.727	0.851	0.631	1.704	0.257
		p-value	<<0.001	<<0.001	<<0.001	<<0.001	<<0.001	0.001	<<0.001	0.119
		Adjusted R^2	0.416	0.403	0.285	0.171	0.165	0.123	0.303	0.018
L5	Flexion Moment	Intercept	363.762	341.320	504.238	140.681	303.432	305.197	452.595	142.241
		Slope	-3.687	-2.624	-4.315	0.523	-1.929	-1.508	-2.633	0.413
		p-value	<<0.001	<<0.001	<<0.001	0.041	<<0.001	<<0.001	<<0.001	0.030
		Adjusted R^2	0.411	0.307	0.381	0.039	0.196	0.177	0.250	0.044
	Compression Force	Intercept	2.606	2.755	4.262	3.199	1.684	2.018	-0.040	2.467
		Slope	0.389	0.252	0.187	-0.036	0.680	0.485	1.520	0.190
		p-value	0.111	0.224	0.611	0.844	0.004	0.017	<<0.001	0.287
		Adjusted R^2	0.019	0.006	-0.009	-0.012	0.086	0.057	0.205	0.002

TABLE B4

Statistical outcomes for each GHBMC injury risk and THOR peak load relationship, by GHBMC lumbar level.

			GHBMC Pinj(Lfx) vs. Y			
			50M-UVA- NHTSA	50M-ATDMODEL	AV	RS
T12	Flexion Moment	Intercept	152.812	181.759	252.213	162.032
		Slope	294.040	261.351	372.612	5.672
		Slope p-value	<<0.001	<<0.001	<<0.001	0.768
		Adjusted R^2	0.475	0.561	0.519	-0.011
	Compression Force	Intercept	2.992	2.790	3.640	2.447
		Slope	4.934	4.400	6.838	3.501
		Slope p-value	<<0.001	<<0.001	<<0.001	<<0.001
		Adjusted R^2	0.543	0.600	0.462	0.501
L1	Flexion Moment	Intercept	151.261	180.224	251.386	159.153
		Slope	474.463	423.073	591.395	33.818
		Slope p-value	<<0.001	<<0.001	<<0.001	0.360
		Adjusted R^2	0.331	0.393	0.349	-0.002
	Compression Force	Intercept	2.769	2.639	3.442	2.396
		Slope	9.667	8.198	12.431	5.936
		Slope p-value	<<0.001	<<0.001	<<0.001	<<0.001
		Adjusted R^2	0.563	0.561	0.410	0.387
L2	Flexion Moment	Intercept	152.207	182.830	255.201	152.635
		Slope	620.085	532.639	742.578	119.987
		Slope p-value	<<0.001	<<0.001	<<0.001	0.041
		Adjusted R^2	0.214	0.236	0.208	0.038
	Compression Force	Intercept	2.683	2.627	3.465	2.430
		Slope	13.845	11.042	16.269	7.494
		Slope p-value	<<0.001	<<0.001	<<0.001	<<0.001
		Adjusted R^2	0.444	0.390	0.268	0.234
L3	Flexion Moment	Intercept	188.225	211.643	294.753	154.117
		Slope	331.345	324.052	463.232	165.945
		Slope p-value	0.152	0.087	0.098	0.079
		Adjusted R^2	0.013	0.024	0.021	0.025
	Compression Force	Intercept	3.050	2.954	4.025	2.740
		Slope	15.516	11.736	15.844	6.337

		Slope p-value	<<0.001	0.000	0.003	0.017
		Adjusted R^2	0.211	0.165	0.091	0.056
L4	Flexion Moment	Intercept	175.306	195.707	270.161	149.291
		Slope	497.607	540.038	801.267	222.631
		Slope p-value	0.013	0.001	0.001	0.007
		Adjusted R^2	0.061	0.117	0.117	0.076
	Compression Force	Intercept	2.933	2.859	3.866	2.556
		Slope	15.403	11.764	16.371	8.497
		Slope p-value	<<0.001	<<0.001	0.000	0.000
		Adjusted R^2	0.273	0.219	0.131	0.147
L5	Flexion Moment	Intercept	223.425	242.297	336.560	151.369
		Slope	-121.893	-92.705	-118.375	82.173
		Slope p-value	0.154	0.186	0.255	0.018
		Adjusted R^2	0.013	0.009	0.004	0.055
	Compression Force	Intercept	3.988	3.725	5.375	3.207
		Slope	-0.716	-0.969	-3.486	-0.881
		Slope p-value	0.596	0.397	0.083	0.376
		Adjusted R^2	-0.009	-0.003	0.025	-0.003